SANDIA REPORT
SAND2017-6679
Unlimited Release
Printed June and 2017

Bryan Mound InSAR Analysis, U.S. Strategic Petroleum Reserve

Anna S. Lord

Prepared by
Sandia National Laboratories
Albuquerque, New Mexico 87185 and Livermore, California 94550

Sandia National Laboratories is a multimission laboratory managed and operated by National Technology and Engineering Solutions of Sandia, LLC, a wholly owned subsidiary of Honeywell International, Inc., for the U.S. Department of Energy's National Nuclear Security Administration under contract DE-NA0003525.

Sandia National Laboratories

Issued by Sandia National Laboratories, operated for the United States Department of Energy by National Technology and Engineering Solutions of Sandia, LLC.

Available to DOE and DOE contractors from
U.S. Department of Energy
Office of Scientific and Technical Information
P.O. Box 62
Oak Ridge, TN 37831

Telephone: (865) 576-8401
Facsimile: (865) 576-5728
E-Mail: reports@osti.gov
Online ordering: http://www.osti.gov/scitech

Available to the public from
U.S. Department of Commerce
National Technical Information Service
5301 Shawnee Rd
Alexandria, VA 22312

Telephone: (800) 553-6847
Facsimile: (703) 605-6900
E-Mail: orders@ntis.gov
Online order: http://www.ntis.gov/search

SAND201X-XXXX
Printed June 2017
Unlimited Release

Bryan Mound InSAR Analysis, U.S. Strategic Petroleum Reserve

Anna S. Lord
Geotechnology and Engineering
Sandia National Laboratories
P. O. Box 5800
Albuquerque, New Mexico 87185-MS0706

Abstract

The U.S. Strategic Petroleum Reserve (SPR) is a stockpile of emergency crude oil to be tapped into if a disruption in the nation's oil supply occurs. The SPR is comprised of four salt dome sites. Subsidence surveys have been conducted either annually or biennially at all four sites over the life of the program. Monitoring of surface behavior is a first line defense to detecting possible subsurface cavern integrity issues. Over the life of the Bryan Mound site, subsidence rates over abandoned Cavern 3 have continuously been the highest at the site. In an effort to try and understand the subsurface dynamics, specifically over Bryan Mound Cavern 3, historic interferometric synthetic aperture radar (InSAR) data was acquired and processed by TRE Altamira. InSAR involves the processing of multiple satellite synthetic aperture radar scenes acquired across the same location of the Earth's surface at different times to map surface deformation. The analysis of the data has the ability to detect millimeters of motion spanning days, months, year and decades, across specific sites. The intent in regards to the Bryan Mound site was (1) to confirm the higher subsidence rates recorded over abandoned Cavern 3 indicated by land survey and (2) understand the regional surface behavior. This report describes the InSAR analysis results, how those results compare to the historical collection of land survey data, and what additional information the data has provided towards understanding the response recorded at the surface.

TABLE OF CONTENTS

FIGURES

TABLES

NOMENCLATURE

Abbreviation	Definition
InSAR	Interferometric satellite aperture radar
SPR	Strategic Petroleum Reserve

1. INTRODUCTION

The U.S. Strategic Petroleum Reserve (SPR) is a stockpile of emergency crude oil to be tapped into if a disruption in the nation's oil supply occurs. The SPR is comprised of four salt dome sites located within Texas and Louisiana (Figure 1). Subsidence surveys have been conducted either annually or biennially at all four sites over the life of the program. Monitoring of surface behavior is a first line defense to detecting possible subsurface cavern integrity issues. Over the life of the Bryan Mound site, subsidence rates over abandoned Cavern 3 have continuously been the highest at the site (Osnes, 1995 (pp 46-48); Bauer, 1999 (pg 8); Lord, 2007 (pp 7-8); Lord, 2009 (pp 8-9)).

In 1982, with the initiation of the Bryan Mound subsidence program, 92 monuments and markers were established for elevation monitoring. Over the years, monuments and markers were destroyed for various reasons and seldom re-established. In 2010 twelve new monuments were added to the site and three previously destroyed monuments were re-established. Five of those monuments were installed over the large expanse of abandoned Cavern 3. In addition, bolts were drilled and tapped into the well head flanges in order to ensure consistent measurements are maintained from year to year. In 2013 a GPS and tiltmeter system was installed over Cavern 3 to continuously monitor ground elevation, well head tilt and surface tilt over and around the perimeter of the cavern.

Surveys were initially conducted annually until 1992 and where then shot every other year until 2009 for budgetary reasons. After 2009 annual surveys were re-established to both ensure quality assurance of the data being collected, as well as improving the ability to monitor the integrity of the site in real time.

However, even at an annual frequency many inconsistencies are introduced in the data and are difficult to eliminate because the spatiotemporal resolution is so low. Since the initiation of the subsidence program monuments have been destroyed, reset, elevation measurements taken at imprecise locations. This is in addition to the challenge of reference benchmarks that are continuously sinking along the Gulf Coast. These continued issues make it difficult to understand the real-time surface behavior. In addition, between the occurrence of an annual surface survey, it is possible that a cavern could lose integrity and collapse within the year seemingly without warning. In contrast interferometric synthetic aperture radar (InSAR) offers a high density of data collected at a high frequency, anywhere from monthly to bi-weekly, which allows for greatly improved temporal resolution monitoring of surface deformation behavior.

In an effort to try and understand the subsurface dynamics, specifically over Cavern 3, historic interferometric synthetic aperture radar (InSAR) data was acquired and processed by TRE Altamira. InSAR involves the processing of multiple satellite synthetic aperture radar scenes acquired across the same location of the Earth's surface at different times to map surface deformation. The analysis of the data has the ability to detect millimeters of motion spanning days, months, year and decades, across specific sites. The intent in regards to the Bryan Mound site was (1) to confirm the higher subsidence rates recorded over abandoned Cavern 3 indicated by land survey and (2) understand the regional surface behavior. This report describes the InSAR analysis results, how those results compare to the historical collection of land survey data, and

what additional information the data has provided towards understanding the response recorded at the surface.

Figure 1. Location map of the U.S. Strategic Petroleum Reserve sites.

2. SALT DOME AND CAVERNS

Understanding the geology of the salt dome and the geometry and location of the caverns within will lend towards better understanding the surface deformation trends recorded at the surface. Bryan Mound is one of many salt domes along the Gulf Coast that is overlain by a caprock. The dome contains 21 caverns.

The caprock is generally circular in shape. The shallowest caprock elevation documented is at elevation of -682 ft. MSL, which is located towards the northwest region of the caprock. In general, the caprock appears to be divided into two regions. These regions are separated by a possible boundary shear zone trending from northeast to the southwest. Within each region, additional boundary shear zones may be present.

The greatest thickness of caprock is over the northwest region with a thickness exceeding 400 ft. (Lord, 2007). The caprock has been characterized in several reports as having three units (Hogan, 1980; Kennedy, 1926). The three-unit division of caprock is very typical in Gulf Coast Salt Domes. Hogan (1980) describes the caprock as follows:

- Unit 1 (uppermost) consists of limestone with water or sulphur-filled pore space.
- Unit 2 (middle) is a transition zone and consists of limestone, gypsum, sulphur and anhydrite.
- Unit 3 (lowermost) consists of anhydrite.

Sulphur deposits are dominant within the middle unit. Crystalline sulphur is found within these voids, along fractures, and as stalactites and plates. Bryan Mound was mined for sulphur by the Frasch process creating large voids that later can collapse and contribute to surface subsidence (Kirby and Lord 2015). Figure 2 displays the caprock and 1935 sulphur ore map. These regions were mined for ore and hence have experienced greater surface subsidence.

The salt dome is basically cylindrical and flat across the top, with virtually no relief (See Figure 3). The shallowest documented salt intercept is at an elevation of -1043 ft., and is located in the center of the dome. To the west, structure contours suggest an isolated region of salt, even though the general topography has not changed. This isolated zone correlates with the thickest part of the caprock, suggesting this region of the dome has experienced the most recent movement of salt upward. Bryan Mound salt dome is heterogeneous and contains more impurities than any of the other three SPR domes. Bryan Mound has anhydrite ($CaSO_4$) concentrations that average between 10 to 20% along with inclusions of shale and sylvite (KCl).

There are 21 caverns within the Bryan Mound salt dome. Figure 2 and 3 show their locations within the salt dome. Five of the caverns, purchased with the property, had previously been leached for brining purposes and the leaching was uncontrolled resulting in a host of relatively large, odd shaped caverns. Four of those caverns are currently being used for oil storage. DOE leached the remaining 16 caverns and all are cylindrical in shape. Creating voids within the dome will manifest as subsidence at the surface.

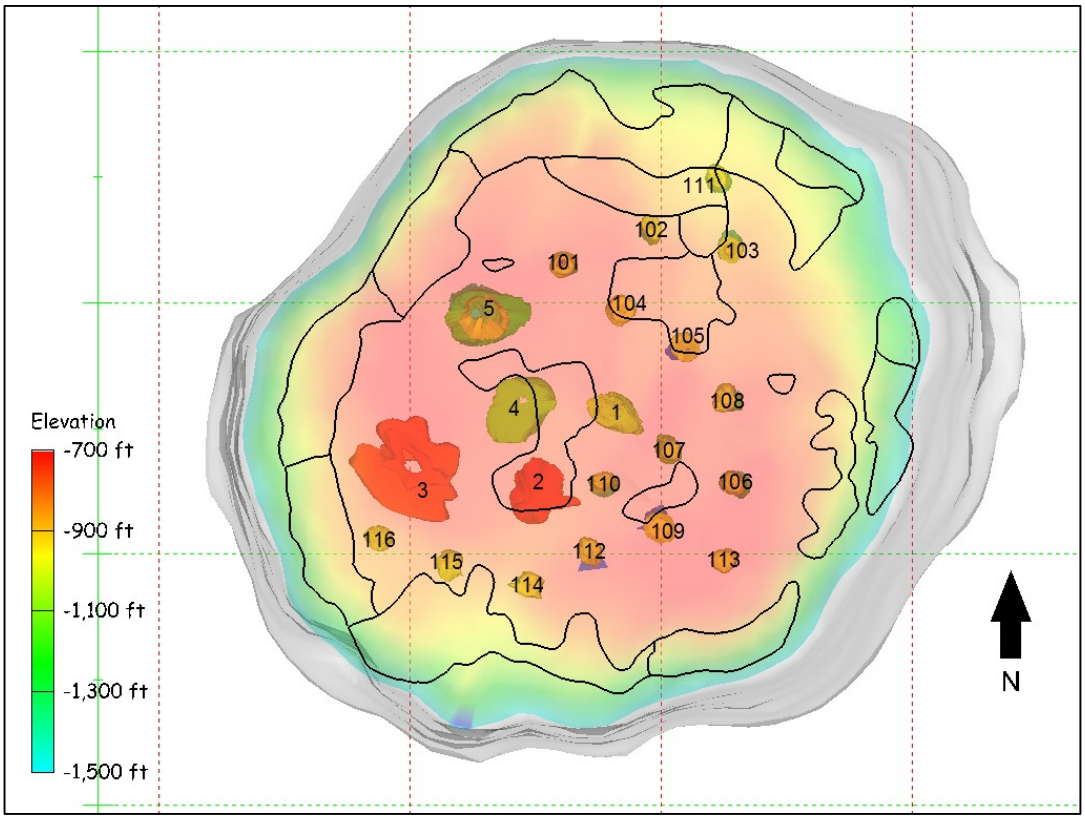

Figure 2. The Bryan Mound caprock map with location of underlying storage caverns. 1935 sulphur ore reserves outlined in black.

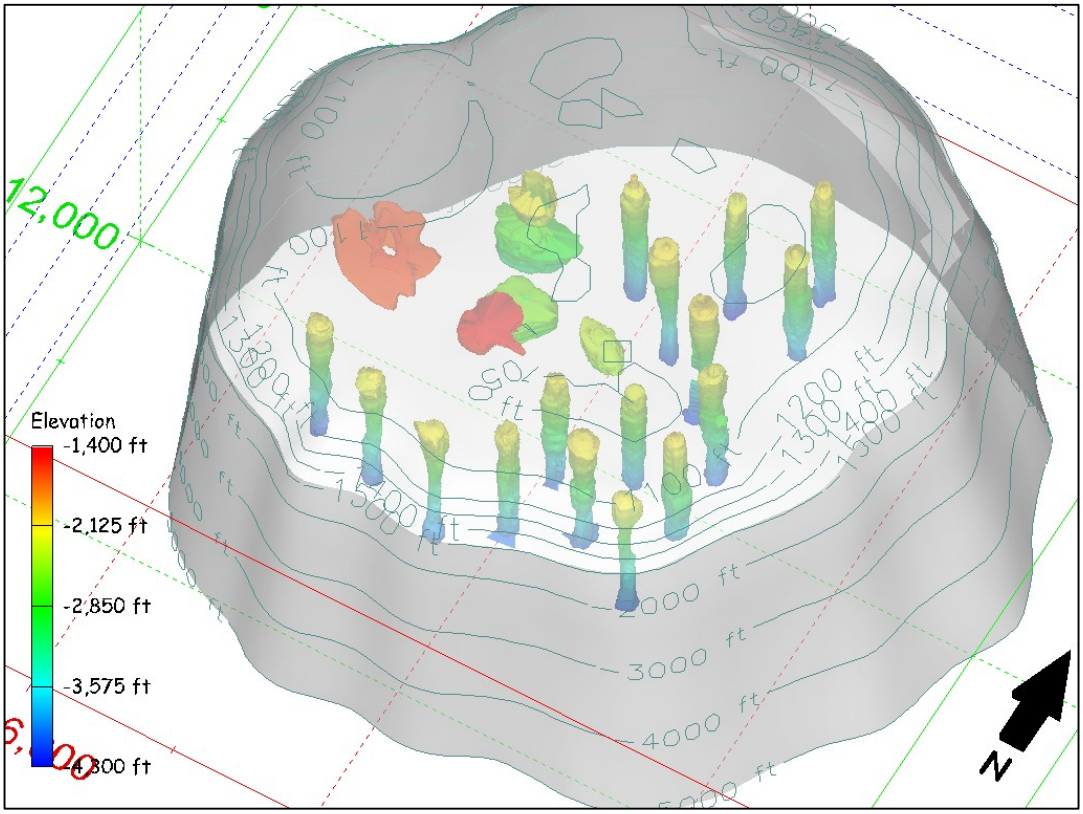

Figure 3. Bryan Mound salt dome and location of underlying storage caverns.

3. SUBSIDENCE

Measuring subsidence rates is one tool to monitor cavern integrity. Typically, cavern closure is expressed at the surface as subsidence. Average site subsidence rates over the life time of the site are displayed in Figure 4. Negative rate indicates subsidence whereas a positive rate indicates uplift. The latest deformation rates are -0.045 ft./yr., which is higher than expected. But, as the plot demonstrates, a saw tooth pattern has been typical for this site, hovering below and above average rates over the years. A cause for this pattern is likely do to erroneous surveys, and supports the acquisition of InSAR data to hopefully get a more realistic picture of the actual trend. However, from year-to-year a consistent trend does persist indicating the highest subsidence rates occur over abandoned Cavern 3, while the lowest rates are measured over the NE corner of the cavern field.

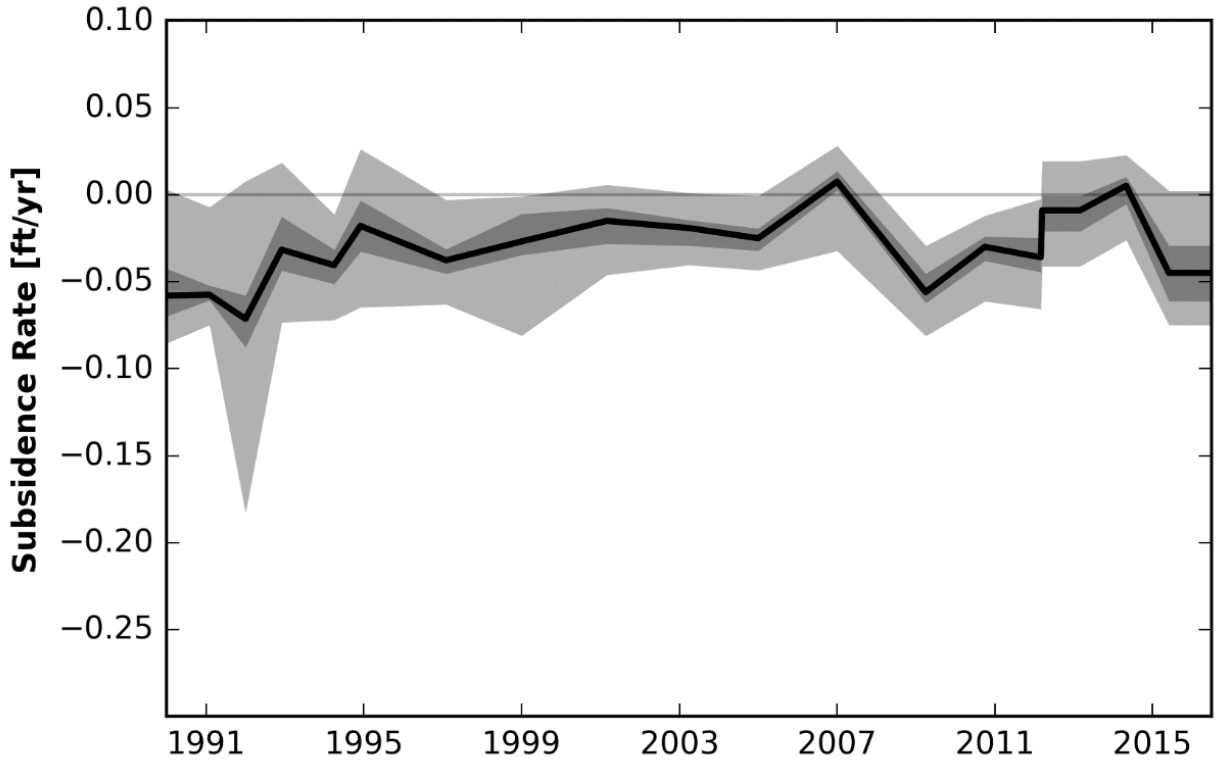

Figure 4. Plot of average subsidence rates over the history of the Bryan Mound program. The black line indicating the median subsidence rate and the darker grey area representing the upper 75th and the lower 25th percentiles. Lighter grey region shows the extents of the 10th and 90th percentiles.

Subsidence rates over abandoned Cavern 3 have continuously been the highest and were first noted in 1995 (Osnes, 1995) and the deviation from average has prompted DOE to install a continuous monitoring program. Average subsidence rates over Cavern 3 have fluctuated between -0.05 ft./yr. and -0.02 ft./yr. over the history of the subsidence program. The GPS unit installed at the well head records a rate of -0.02 ft./yr.

A series of three tiltmeters monitor both well head tilt and surface tilt around the perimeter of the cavern. Both in-ground tiltmeters tilt towards the southeast, whereas the wellhead tiltmeter is essentially stable with little or no tilt. In addition, the highest subsidence rate measured over Cavern 3 is located in the southeast region of the cavern (Lord, 2014).

4. INSAR RESULTS

Since the land surveys are not always consistent from one year to the next and are sporadically deemed erroneous the acquisition of interferometric synthetic aperture radar (InSAR) was acquired to hopefully get a realistic idea of ground deformation rates, as well as perhaps get a better understanding of the ground behavior occurring over Cavern 3 and what that might mean. InSAR obtains a higher density and frequency of data collection.

Three different InSAR data sets were acquired and analyzed to examine differences in results, and provide recommendations for the potential future monitoring of the Bryan Mound site. Data was collected from both the Cosmo-SkyMed (CSK) and Sentinel (SNT) satellites. The data sets used and the period covered are listed in Table 1.

Table 1. Listing of satellite data acquired by satellite, acquisition frequency, and acquisition period.

Satellite	Geometry	No. of Images	Density of measurement points	Repeat Interval	Acquisition Period
CSK	Ascending	40	7811	8-days	10/17/2015-10/03/2016
CSK	Ascending	23	5058	16-days	10/17/2015-09/25/2016
SNT	Descending	25	736	12-days	12/26/2014-11/3/2015

TRE Altamira produced a technical report that was delivered to Sandia National Laboratories on December 2, 2016 detailing their analysis and results. The report is included as Appendix A and presents the results in detail. This Sandia report is not meant to restate the results, but offer insight into what geologic or operational influences may be contributing to the noted surface behavior. After reviewing the three data sets it was decided that the CSK 8-day repeat results displayed the highest precision. The data contained the highest number of images and highest density of measurement points. Results discussed below will be in reference to the CSK 8-day analysis. See Appendix A for details on all three data sets collected and analyzed.

Figure 5 displays the displacement rate between October 2015 and October 2016. Visually the southwestern region displays the greatest displacement rates whereas the northeastern region shows the least. The site average displacement as a whole is “mild” and within the expected range. The results are listed in Table 2.

Acceleration rate is used to identify non-linear trends in the deformation time series, as well as areas where the deformation rate is increasing or decreasing over time. Negative accelerations (red) indicate an increase in downward movement. Negative rates can be seen across the entire site, but are more acute in the areas surrounding abandoned Cavern 3 and the storage tanks (Figure 6). The increase or decrease in acceleration around the tanks themselves is most likely caused by the filling and emptying of the tanks.

Profiles can be selected to display the data as surface displacement through time between October 2015 and October 2016. Figure 7 displays a cross section through Cavern 3 to the eastern edge of the site. This particular transect was selected to visually emphasize the change in

rate between Cavern 3 and the rest of the site towards the east.

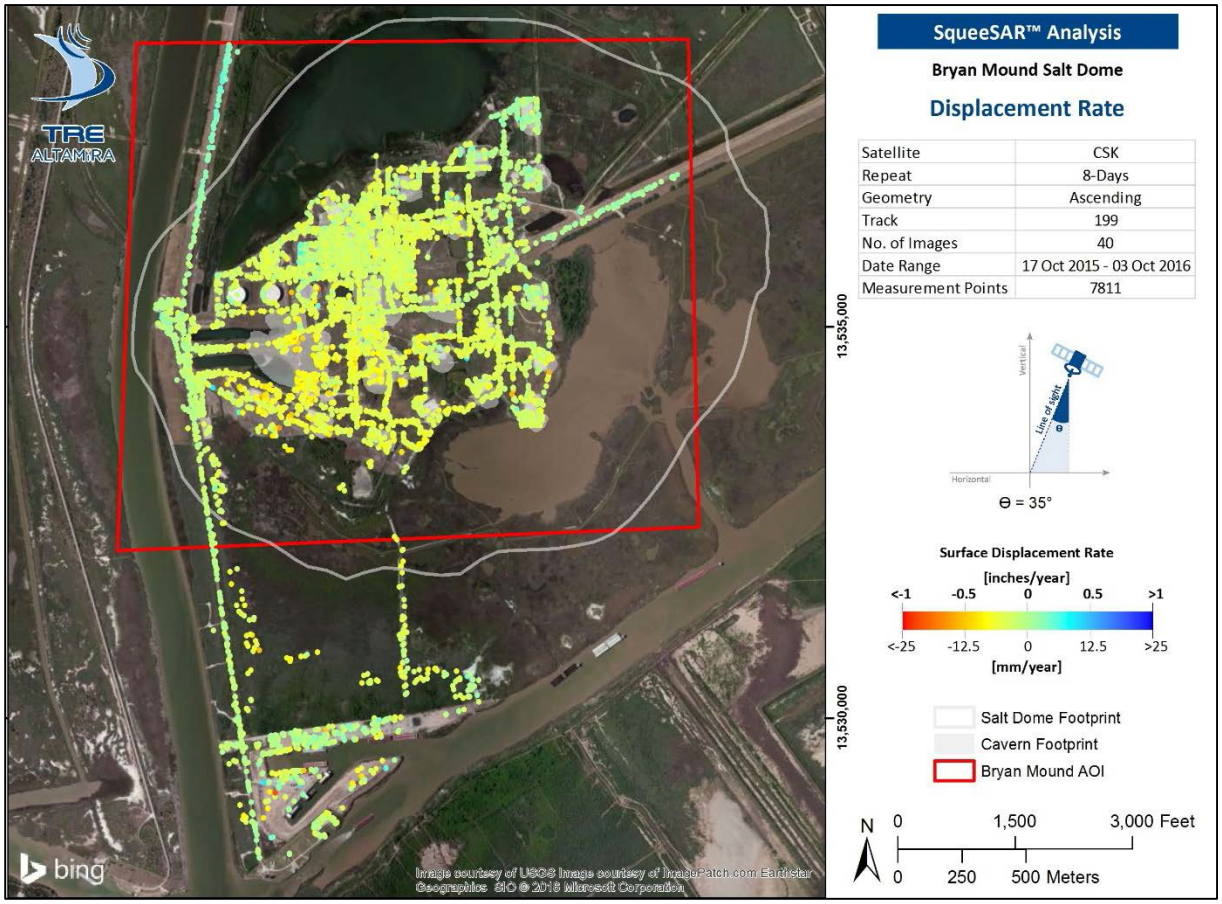

Figure 5. Annual surface displacement rates obtained from the CSK 8-day analysis.

Table 2. Averaged deformation rate of select caverns.

	Avg. Displacement mm/yr	Avg. Displacement ft/yr
Site wide (entire dome)	3.3	0.01
Southwestern region		
Cavern 3	6.6	0.02
Cavern 2	5.7	0.02
Cavern 116	5.9	0.02
Cavern 115	5.1	0.02
Cavern 114	6.3	0.02
Northeastern region		
Cavern 111	0.7	0.00
Cavern 102	1.2	0.00
Cavern 103	0.2	0.00

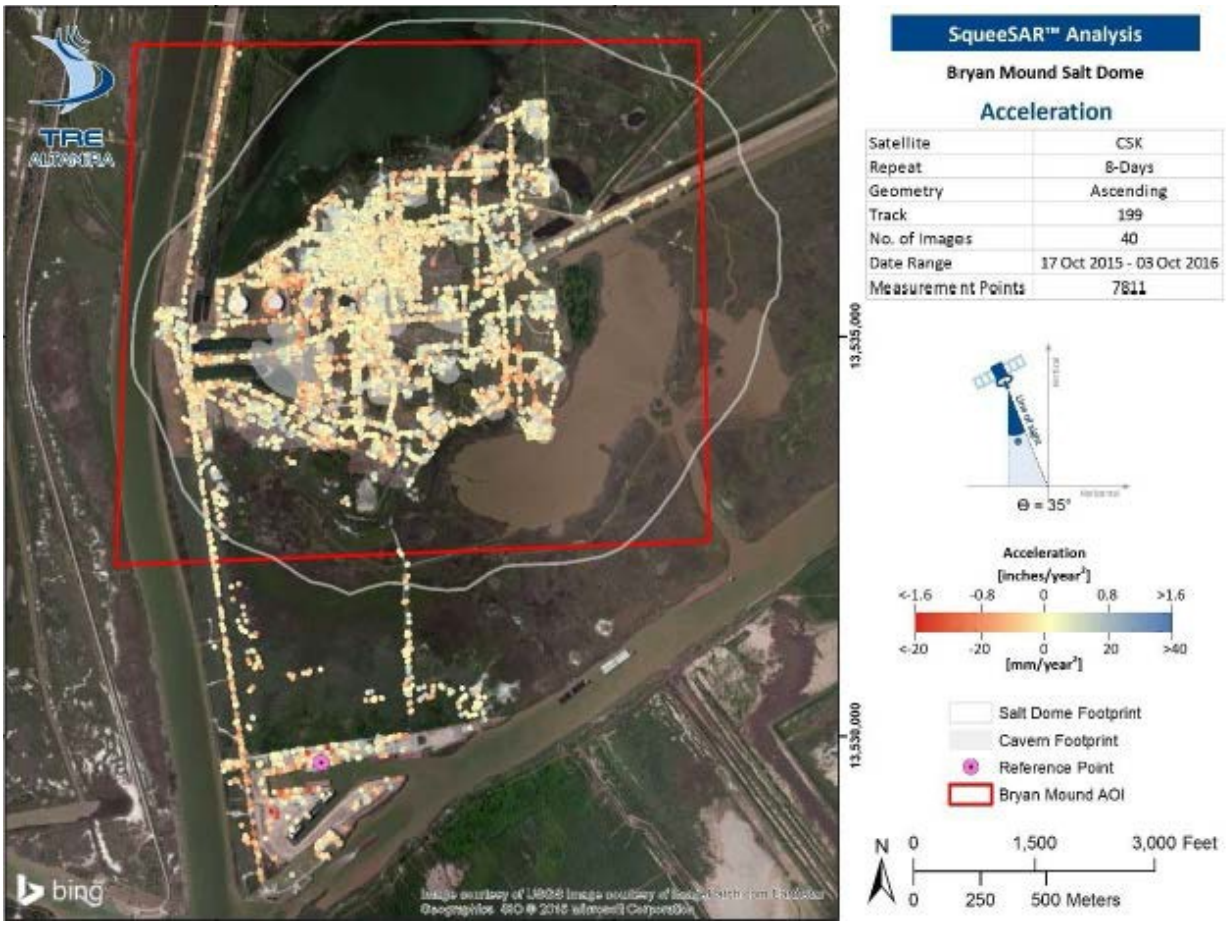

Figure 6. Acceleration rates obtained from the CSK-8 day analysis.

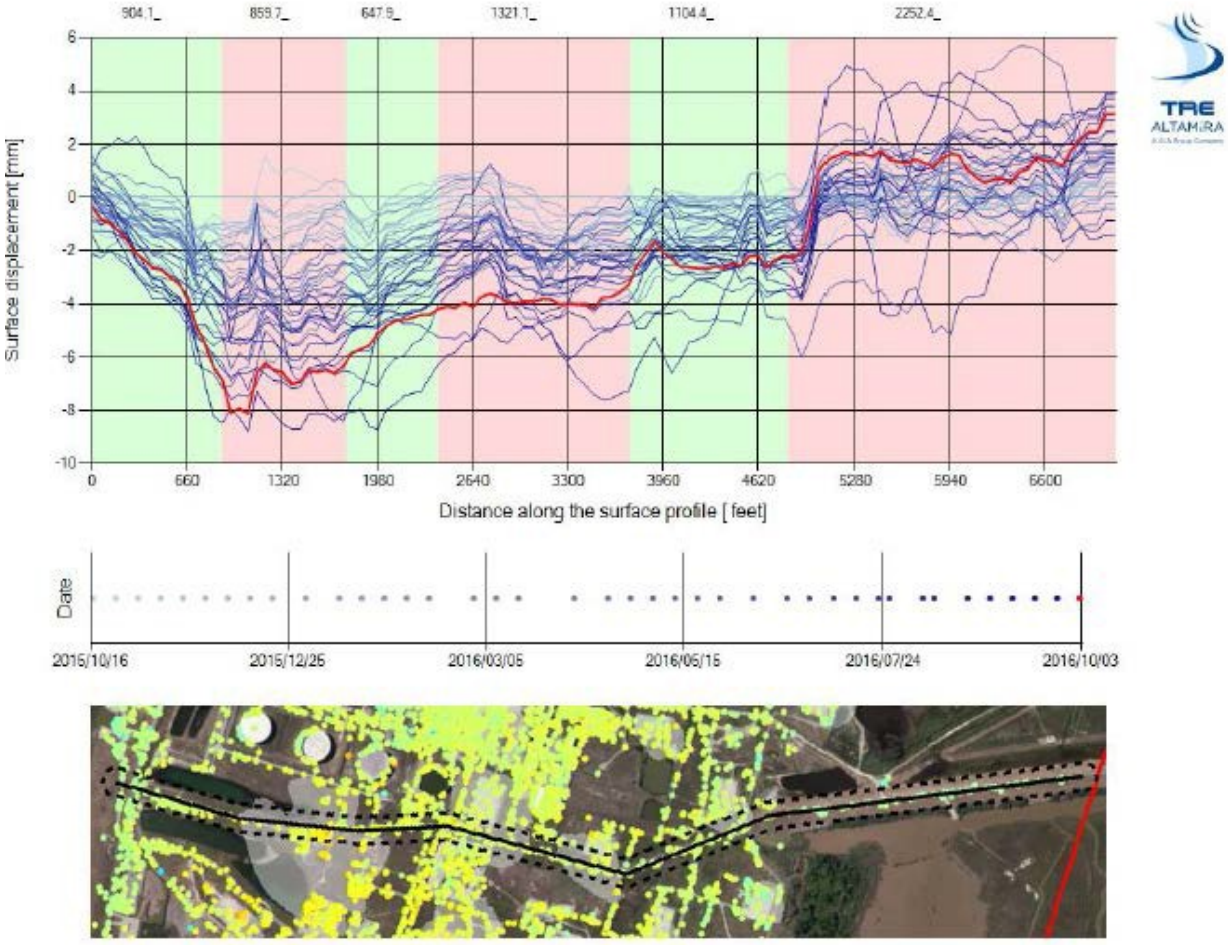

Figure 7. Evolution of the selected surface profile. The profile highlighted in red corresponds to the final image of the data stack.

5. DISCUSSION

InSAR indicates that the southwestern portion of the dome is subsiding at a higher rate than the rest of the site, which encompasses caverns 3, 2, 116, 115, and 114. Comparison of the land survey results with the InSAR results adds credence to the subsidence trend observed. Figure 8 displays a series of subsidence plots spanning the history of the SPR subsidence land survey program. What can be discerned from these maps is that in general higher subsidence rates occur across the southern and southwestern portion of the site whereas the subsidence rates are lowest across the northeastern region of the site. In particular, the greatest subsidence rate is over abandoned Cavern 3. The similarity in general trend corroborates the recorded ground behavior from both data acquisition methods. What the InSAR provides is a plethora of data over a short time frame allowing a reduction in 'noise' and the ability to analyze actual subsidence trends. Possible contributing factors to the higher rates recorded by InSAR are discussed within this section. Aspects examined were (1) geology, (2) creep rates, (3) cavern depth, size, and geometry, (4) cavern history/status, (5) sulphur mining impacts, and (6) work over impacts.

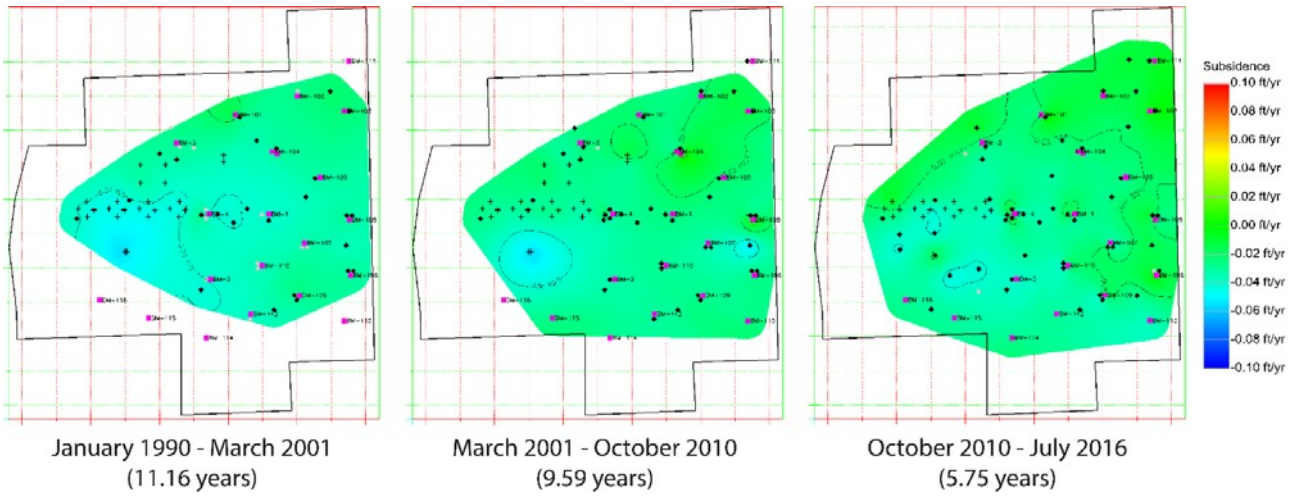

Figure 8. Calculated Bryan Mound subsidence rates over time from the annual subsidence surveys. The cooler colors indicate greater subsidence while the warmer colors represent less subsidence. The SPR well locations are labeled with pink squares. Survey monuments are depicted as diamonds and survey markers used are shown as crosses. Grey survey monument/marker indicate that the survey location was unavailable for at least one of the two surveys used to create the map.

Bryan Mound is heterogeneous and is comprised of sections with varying salt creep rates. Table 3 lists the most recently calculated creep rates. Note that caverns 106, 114, and 115 have the highest creep rates. Cavern 116 is average and Cavern 2 exhibits the slowest creep rate. Cavern 3, being abandoned does not have data available for creep rate. Higher creep rate may explain the higher subsidence rates exhibited over caverns 115, and 114. The higher subsidence rates at Cavern 116 may be explained by its proximity to caverns 115 and 3. Creep rate does not explain the behavior documented over Cavern 2.

Table 3. Calculated cavern closure rates for Bryan Mound caverns between 2008-2014.

Cavern	Closure Rate, bbl/yr	Cavern	Closure Rate, bbl/yr
101	11,790	111	12,973
102	11,833	112	15,463
103	18,710	113	17,004
104	9,748	114	20,028
105	5,573	115	26,470
106	24,716	116	10,995
107	8,172	1	3,071
108	7,055	2	346
109	12,241	4	14,535
110	6,525	5	15,604

Cavern 3 exhibits the highest subsidence at 6.6 mm/yr. Cavern history (Giles, 1978; KAI, 1980) records indicate that the cavern is characterized by a large horizontal expanse (~1600 ft.), thin salt roof, and located at a fairly shallow depth. Logging also indicates that a void in the caprock, over the cavern, is present from 730' to 1036' (306' in height). There is debate between the two reports whether the cavern is or is not in hydraulic communication with the caprock and surrounding salt flank. What can be said is that the pancake shape of the cavern is not a stable configuration and that there is evidence that caprock is collapsing within the caprock void

directly above the cavern (KAI, 1980). A loss in integrity with either structural cavity could certainly cause a response in surface subsidence.

The surface subsidence recorded above Cavern 2 presents more of a mystery. This cavern's calculated closure rates are the lowest out of all 20 storage caverns; this is due in part to the shallow depth of the cavern, which means that the differential stress between lithostatic and internal cavern pressures is less than other caverns, resulting in lower strain rate due to creep. However, of interest, the cavern has been emptied of oil over the past 2 years and evidenced by the historic pressure data, shown in Figure 9, there have been periods where the cavern has been at a lower pressure. Also, its proximity to Cavern 3 (perhaps leaking to caprock), 114 and 115 (caverns with fast closure rate), the middle of the site where maximum subsidence tends to be, and at a shallow depth near the top of the dome (Table 4) would all tend to contribute to the surface over Cavern 2 having higher subsidence than other areas.

Table 4. Cavern shape and parameters.

Cavern	Roof thickness	Top of Cavern	Cavern Height	Cavern Diameter
2	365	1450	225	600
3	394	1520	195	1350
All Phase 2 caverns		2000+	~2000	200

The sulphur ore map was reviewed and mining may have occurred over the Cavern 2 region (Figure 1). The sulphur mining process could certainly lead to greater subsidence rates. However, when looking at the site as a whole, there has also been significant sulphur mining over the northeastern portion of the site and subsidence rates are at the lowest in that region. The impact of sulphur mining is not conclusive.

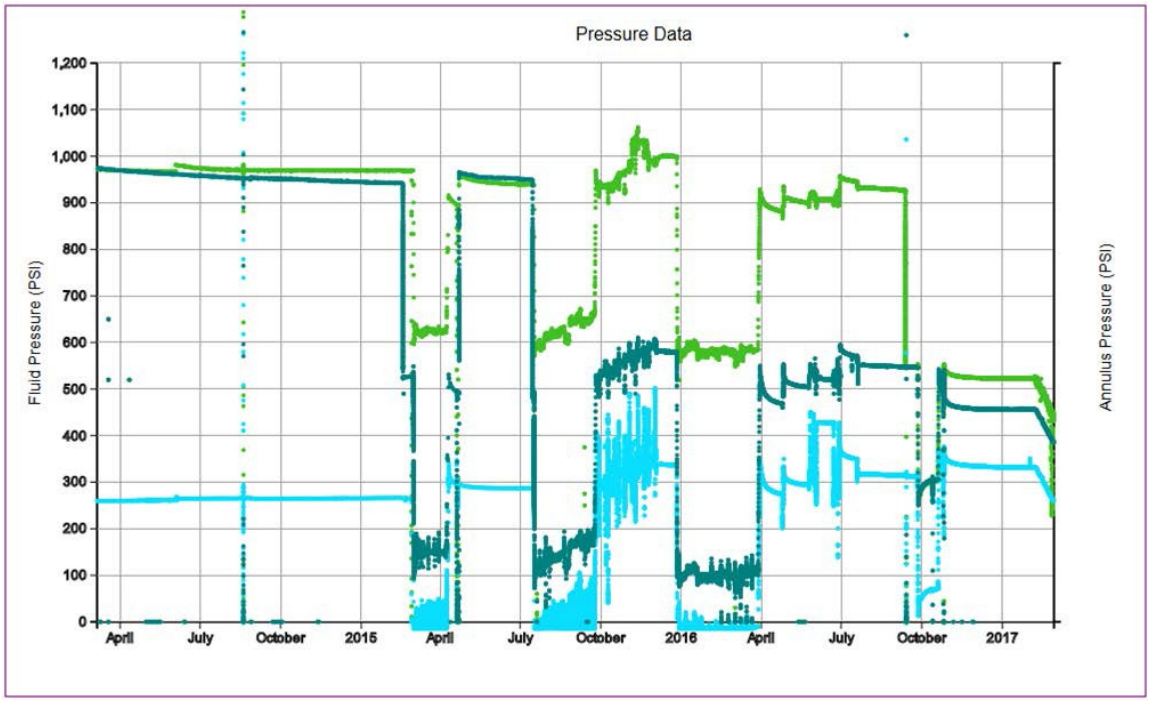

Figure 9. Bryan Mound Cavern 2 plot of oil and brine pressures. Light green – oil pressure well 2A; dark green – oil pressure well 2; cyan- brine pressure well 2A.

Often a series of workovers can cause a temporary increase in subsidence and once a cavern is re-pressurized the ground will rebound and typical subsidence rates will resume. The workover schedule was reviewed during the window of InSAR collection and none of the cavern locations measuring the higher subsidence were under a workover during that time.

6. SUMMARY

In summary, in an effort to try and understand the subsurface dynamics, specifically over Cavern 3, historic interferometric synthetic aperture radar (InSAR) data was acquired. The high density and frequency of data collection allows for real-time monitoring of surface deformation behavior. Three data sets were analyzed and the Cosmo-SkyMed (CSK) satellite on an 8-day repeat gave the greatest precision in results.

Analysis and interpretation of the CSK data collected between October 2015 and October 2016 every 8 days indicate that the highest subsidence rates are occurring over caverns 2,3, 114, 115, and 116, all of which are located within the southwestern portion of the site. With the exception of Cavern 2, the southwestern region of the site exhibits high cavern closure rates. Cavern 3 and Cavern 2 were created from brining operations and due to integrity concerns Cavern 3 was abandoned. A clear cause for the higher subsidence rates over Cavern 2 cannot be discerned, but most likely the cause is a combination of factors, shallow depth, vicinity to Cavern 3, location in the middle of the site, and proximity to the higher creeping caverns.

The ground surface above Cavern 3 continues to exhibit the greatest subsidence rate. This trend has been noted for years by the annual land surveys and the current InSAR data set. InSAR images are continuing to be collected through May 2017 and an updated analysis report is due to Sandia in June 2017. The next data set collected will be for a 2D analysis. 2D analysis allows for observation of ground deformation in both the true vertical and east/west direction. In combination with the previous data set a refinement in the results can be made.

7. REFERENCES

Bauer, S. J. 1999. Analysis of Subsidence Data for the Bryan Mound Site, Texas. SAND99-1739. Albuquerque, NM: Sandia National Laboratories.

Giles, H. N. and R. E. Smith. 1978. Bryan Mound Cavern 3, memorandum from H.N. Giles (SPRPMO) to J. R. Deluca, November 7, 1979.

Hogan, R.G. 1980. "Strategic Petroleum Reserve (SPR) Geological Site Characterization Report, Bryan Mound Salt Dome", SAND80-7111. Sandia National Laboratories, Albuquerque, NM, October 1980.

KAI (Keplinger and Associates, Inc.). 1980. Report of Investigations on Cavern #3 Bryan Mound Strategic Petroleum Reserve Freeport, Texas. Report for Dravo Utility Constructors, Inc. and U.S. DOE New Orleans, Louisiana, August 30, 1980.

Kirby, C. K. and A. S. Lord. 2015. Sulphur Extraction at Bryan Mound. SAND2015-6827. Sandia National Laboratories, Albuquerque, NM.

Kennedy, W., 1926, "The Bryan Heights Salt Dome, Brazoria County, Texas", American Association of Petroleum Geologists Special Volumes – SP 1 – Geology of Salt Dome Oil Fields, pp. 678-690.

Lord, A.S. 2014. May 2014 Bryan Mound Subsidence Analysis. Letter report to P. Tilly DOE SPR PMO, September 11, 2014.

Lord, A.S. 2009. April 2009 Bryan Mound Subsidence Analysis. Letter report to W. Elias DOE SPR PMO, November 16, 2009.

Lord, A. S. 2007. January 2007 Bryan Mound Subsidence Analysis. Letter report to R. Myers DOE SPR PMO, April 11, 2007.

Lord, A.S., 2007, "An Updated Three-Dimensional Site Characterization Model of the Bryan Mound Strategic Petroleum Reserve Site, Texas" p.35.

Osnes, J.D. 1995. *Update to Subsidence Analyses of Strategic Petroleum Reserve Sites for Fiscal Years 1993 and 1994*. Topical Report RSI-0590. Rapid City, SD: RE/SPEC

8. APPENDIX A

“SqueeSAR Analysis of Ground Movement over Bryan Mound”

Technical report submitted to A. Lord SNL by TRE Altimara on December 2, 2016

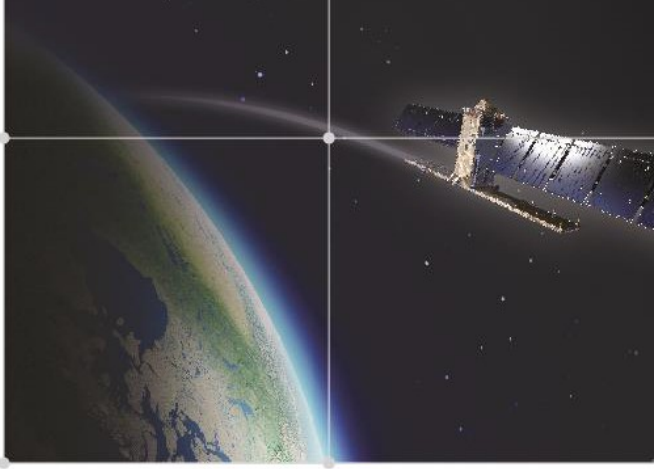

SqueeSAR Analysis of Ground Movement over Bryan Mound

Technical Report

2 December 2016

TRE ALTAMIRA

A CLS Group Company

Report specifications

Client:

Anna Snider Lord
Sandia National Laboratories
PO Box 5800 MS1485
Albuquerque, New Mexico
87145-1485

Reference:

Technical Report	SqueeSAR™ Analysis of Ground Movement over Bryan Mound
TRE ALTAMIRA Job Order:	JO16-3053
Client Contract Number:	1727113
Client Order Date:	2016/09/13

Prepared by:

TRE ALTAMIRA

Authors:	Danielle Ambs
Verified by:	Jessica Morgan
Approved by:	Giacomo Falorni
Date:	2016/12/02
Version:	1.0

Executive Summary

TRE Altamira Inc. was contracted by Sandia National Laboratories (Sandia) to analyze ground stability over the Bryan Mound salt dome with the aim of capturing current movement trends, and to provide recommendations for an InSAR monitoring program going forward. This report describes the results of three analyses using TRE Altamira's proprietary SqueeSAR™ algorithm and Cosmo-SkyMed (CSK) and Sentinel (SNT) data stacks collected between 17 October 2015 to 3 October 2016, and 26 December 2014 to 3 November 2015, respectively. The following points summarize the key findings and features of this work:

- Mild subsidence was observed over most of the Bryan Mound salt dome. Slightly stronger, more localized deformation was identified within the area surrounding cavern 3.
- Cumulative surface displacement values for the 8-day and 16-day CSK analyses identified maximum subsidence values of -0.7 inches (-18.2 mm) and -0.9 inches (-22.8 mm), respectively. An average rate of -0.1 inches/year (-3.3 mm/year) and -0.2 inches/year (-5.2 mm/year) was found for the 8-day and 16-day studies.
- Results from the analysis of the SNT data identified a similar average displacement rate of -0.2 inches/year (-5.6 mm/year), with as much as -1.3 inches (-32.1 mm) of subsidence observed over the time period analyzed.
- The highest measurement point density (4733.9/mi^2, or 1820.7/km^2) was obtained from the processing of the 8-day CSK stack, vs 3065.5/mi^2 (1181.8/km^2) for the 16-day archive and 446.1/mi^2 (172.0/km^2) for the medium resolution SNT data.
- Animations of ground displacement are provided, and show the evolution of surface deformation over the entire time periods covered by each analysis.

Table of Contents

1. Radar Data

Three separate SqueeSAR analyses have been carried out to examine differences in results, and provide recommendations for the potential future monitoring of the Bryan Mound storage facility using InSAR (Figure 1 & Table 1). The datasets were acquired from Cosmo-SkyMed (CSK) and Sentinel (SNT) satellites.

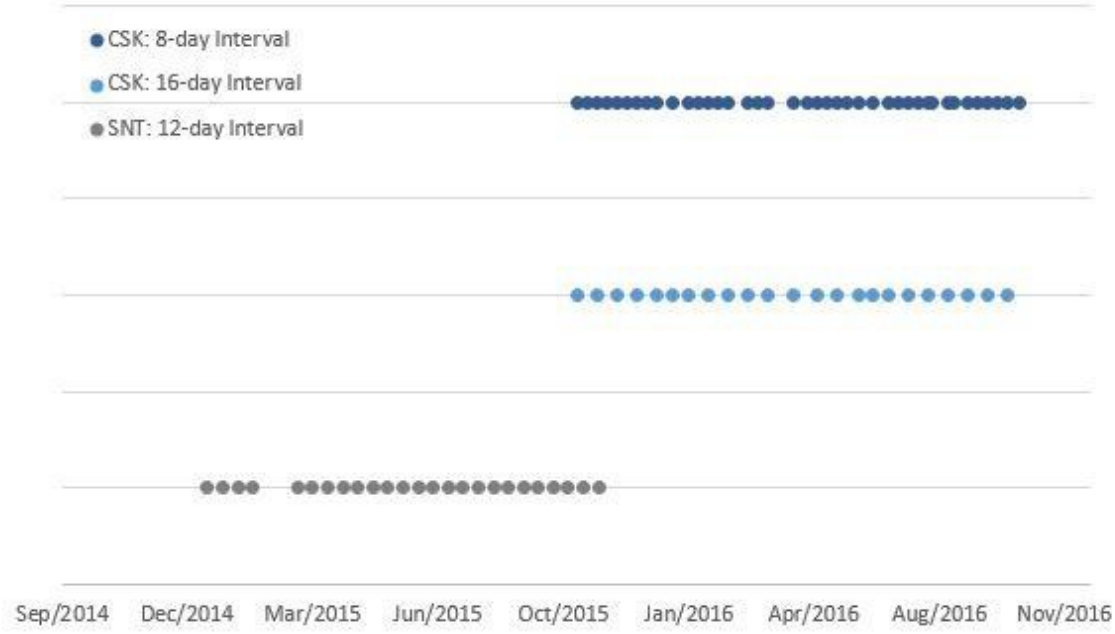

Figure 1: Time period covered by the datasets used the 1D analyses.

Satellite	Geometry	No. of Images	Repeat Interval	Acquisition Period
CSK	Ascending	40	8-Days	17 Oct 2015 – 03 Oct 2016
CSK	Ascending	23	16-Days	17 Oct 2015 – 25 Sept 2016
SNT	Descending	25	12-Days	26 Dec 2014 – 3 Nov 2015

Table 1: Datasets used for SqueeSAR analyses.

The first data set processed contained 40 images acquired by the Italian Space Agency CSK satellite, collected between 17 October 2015 and 03 October 2016 on an 8-day image acquisition schedule (Table 22). Images were collected along track 199 in mode H4-05 from an ascending orbit. The second data set was obtained by subsampling the original CSK archive to a 16-day frequency, leading to the processing of 23 images (Table 33).

The ascending CSK image acquisitions are scheduled to continue in the same configuration going forward into 2017. A second CSK stack has been tasked in the opposing orbit over this site, which started in October 2016 for the upcoming 2D analysis to be completed in May 2017.

8-day CSK Archive Data				
17/10/2015	20/12/2015	09/03/2016	28/05/2016	08/08/2016
25/10/2015	01/01/2016	17/03/2016	09/06/2016	12/08/2016
02/11/2015	13/01/2016	06/04/2016	21/06/2016	24/08/2016
10/11/2015	21/01/2016	18/04/2016	29/06/2016	01/09/2016
18/11/2015	29/01/2016	26/04/2016	07/07/2016	09/09/2016
26/11/2015	06/02/2016	04/05/2016	15/07/2016	17/09/2016
04/12/2015	14/02/2016	12/05/2016	23/07/2016	25/09/2016
12/12/2015	01/03/2016	20/05/2016	27/07/2016	03/10/2016

Table 2: Dates of the 8-day repeat CSK archive images.

16-day CSK Archive Data				
17/10/2015	01/01/2016	17/03/2016	09/06/2016	24/08/2016
02/11/2015	13/01/2016	06/04/2016	21/06/2016	09/09/2016
18/11/2015	29/01/2016	26/04/2016	07/07/2016	25/09/2016
04/12/2015	14/02/2016	12/05/2016	23/07/2016	
20/12/2015	01/03/2016	28/05/2016	08/08/2016	

Table 3: Dates of the 16-day repeat CSK archive images.

The third dataset processed comprises 23 images acquired from the European Space Agency SNT satellite between 26 December 2014 and 3 November 2015 on a 12-day image acquisition schedule (Table 4). Images were collected in interferometric wide swath mode on track 143 in a descending orbit.

The footprint of the SNT scene used for this analysis was shifted north by the satellite provider in November 2015, and as a result does not provide consistent coverage over the Bryan Mound AOI since this switch was made. As image acquisitions with the SNT satellite cannot be commercially tasked, there is a possibility that this satellite will not be available for ongoing monitoring over this area. TRE Altamira has contacted the satellite operator to see if the frame can be shifted south to provide coverage over this site going forward.

12-day SNT Archive Data				
26/12/2014	20/03/2015	19/05/2015	18/07/2015	16/09/2015
07/01/2015	01/04/2015	31/05/2015	30/07/2015	28/09/2015
19/01/2015	13/04/2015	12/06/2015	11/08/2015	10/10/2015
31/01/2015	25/04/2015	24/06/2015	23/08/2015	22/10/2015
08/03/2015	07/05/2015	06/07/2015	04/09/2015	03/11/2015

Table 4: Dates of the 12-day repeat SNT archive images.

2. Area of Interest

The area of interest (AOI) for this analysis can be seen below in Figure 2. The salt dome is located to the west of Freeport, TX and covers 1.65 mi^2 (4.28 km^2). The Bryan Mound storage facility contains 20 active storage caverns and 1 abandoned cavern. Storage caverns are located at depths of 2000 feet (610 m) with the exception of 2 slightly shallower caverns, found at 1400 feet (425 m). The approximate footprints of the caverns and the salt dome can also be seen below.

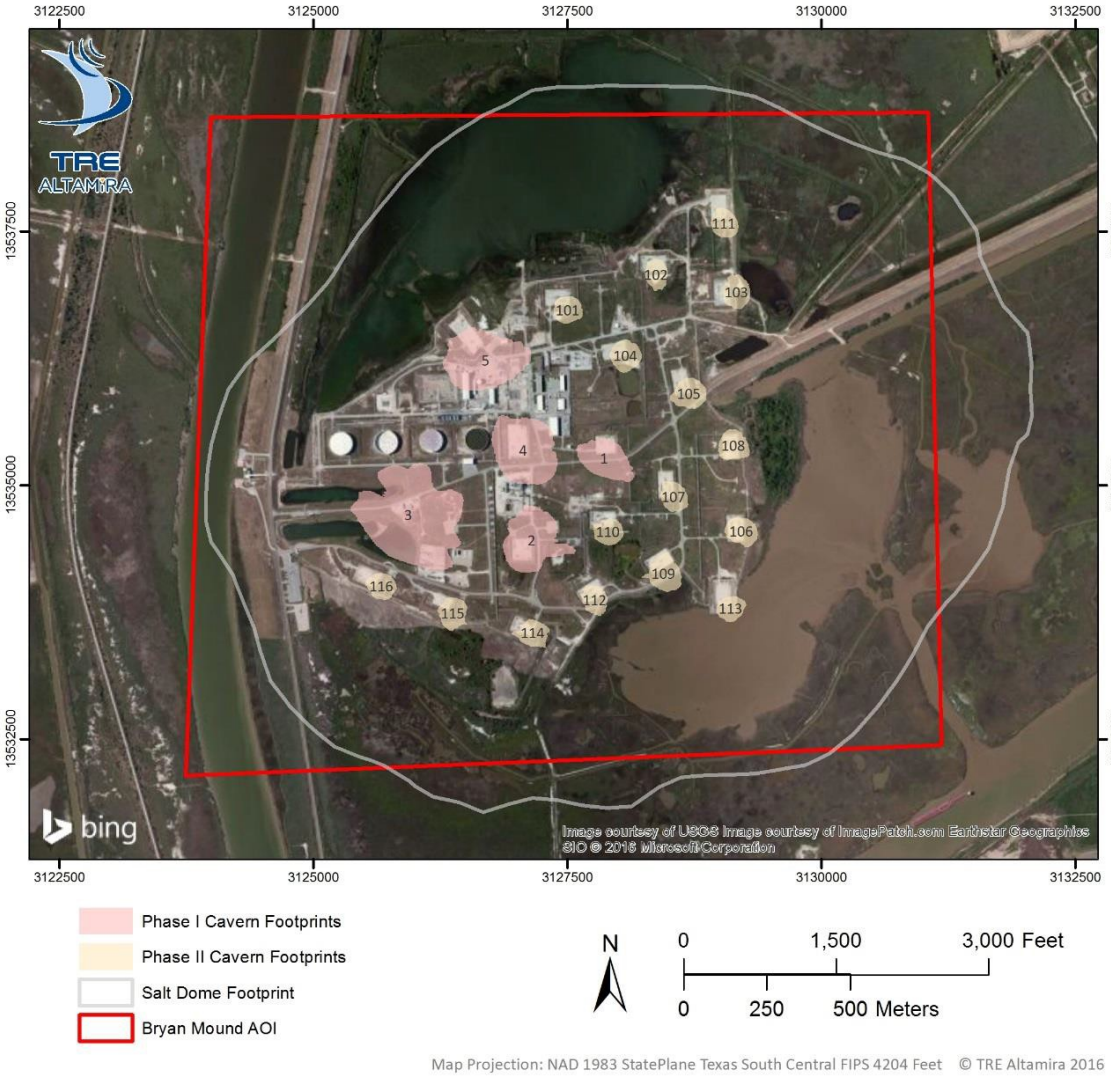

Figure 2: The area of interest (AOI) for the Bryan Mound Salt Dome.

3. Results

3.1. Cumulative Displacement

Cumulative surface displacement measured from the analysis of the 8-day CSK data can be seen in Figure 3. The current processing covers a larger area than the AOI in order to provide context to any movement trends occurring on the salt dome. The location of the reference point for all analyses, as seen below, was selected from an area of infrastructure to the south of the salt dome. More information on the location of reference points can be found in Appendix 1.

Each measurement point corresponds to a Permanent Scatterer (PS) or Distributed Scatterer (DS), and is colour-coded according to the magnitude of total movement. Surface displacement is measured along the line-of-sight (LOS) of the satellite and is represented in both US customary and metric units in the figures below. Negative values (red) indicate surface displacement away from the satellite (e.g. subsidence), while positive values (blue) indicate surface displacement towards the satellites (e.g. uplift). Total surface displacement identified by the CSK 8-day analysis ranged from +0.5 inches (+12.5 mm) to -0.7 inches (-18.2 mm).

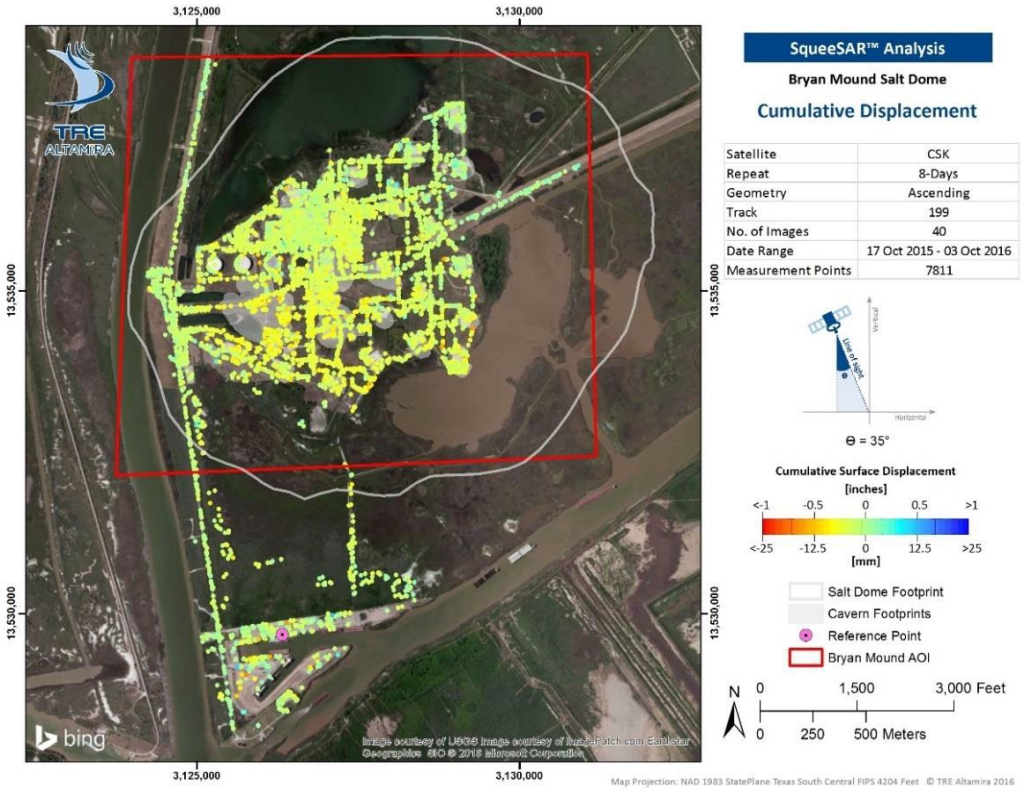

Figure 3: Cumulative displacement obtained from the CSK 8-day analysis.

Cumulative displacement measured from the subsampled, 16-day CSK analysis can be seen in Figure 4. Total surface displacement identified from this analysis ranged from +0.4 inches (+9.7 mm) to -0.9 inches (-22.8 mm). The deformation trends are similar to those observed in the 8-day CSK data.

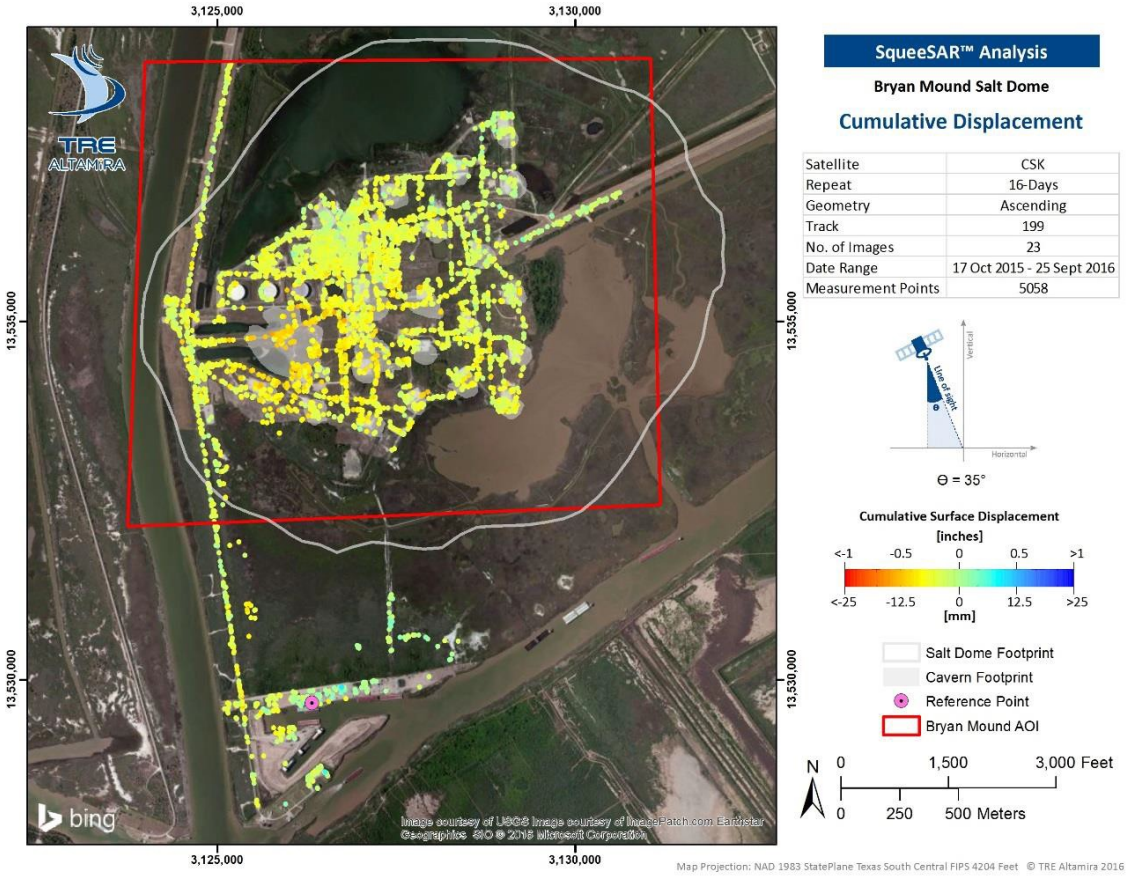

Figure 4: Cumulative displacement obtained from the CSK 16-day analysis.

Comparison of the results obtained from the 8- and 16-day CSK SqueeSAR analyses can be seen in Figure 5. This comparison allows for the visualization of the movement trends identified over the same time period using a different acquisition frequency. Cumulative movement trends identified with these two analyses appear consistent, however slightly stronger deformation values were identified in the 16-day analysis. Average cumulative subsidence values identified from the 8- and 16-day analyses were -0.1 inches (-3.2 mm and -0.2 inches (-5.1 mm), respectively. This difference is most likely due to the smaller number of images used in the 16-day analysis, which means estimates of displacement will be slightly less precise.

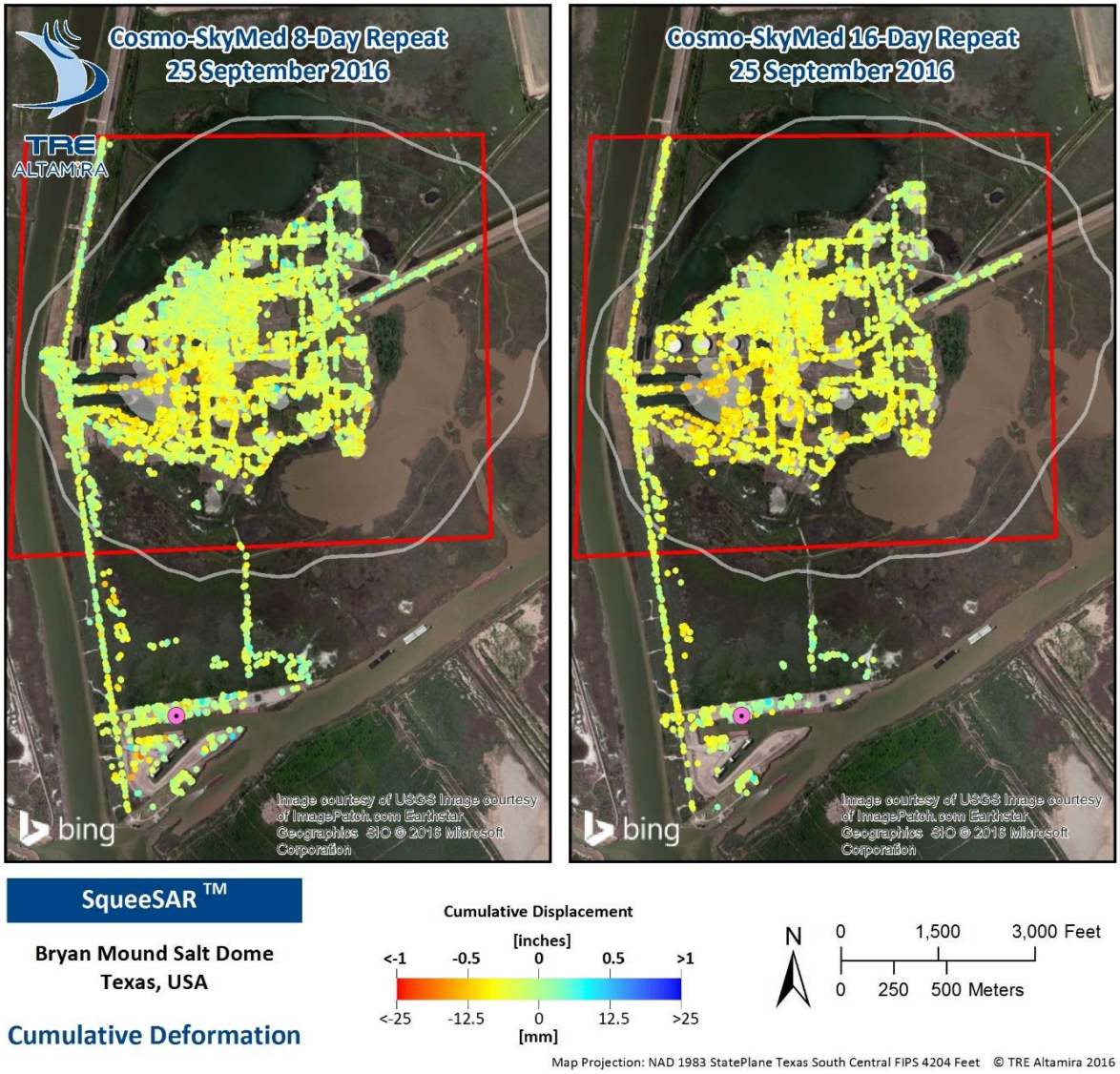

Figure 5: Comparison of cumulative displacement between CSK analyses.

Cumulative displacement measured from the SNT analysis between 26 December 2014 to 03 November 2015, can be seen in Figure 6. Note that this data does not overlap in time with the CSK data. Mild deformation was observed across most of the AOI with the strongest subsidence values identified from the area surrounding cavern 3. Total surface displacement identified by this analysis ranged from +0.6 inches (+14.1 mm) to -1.3 inches (-32.1 mm), with an average cumulative subsidence of -0.2 inches (-4.1 mm).

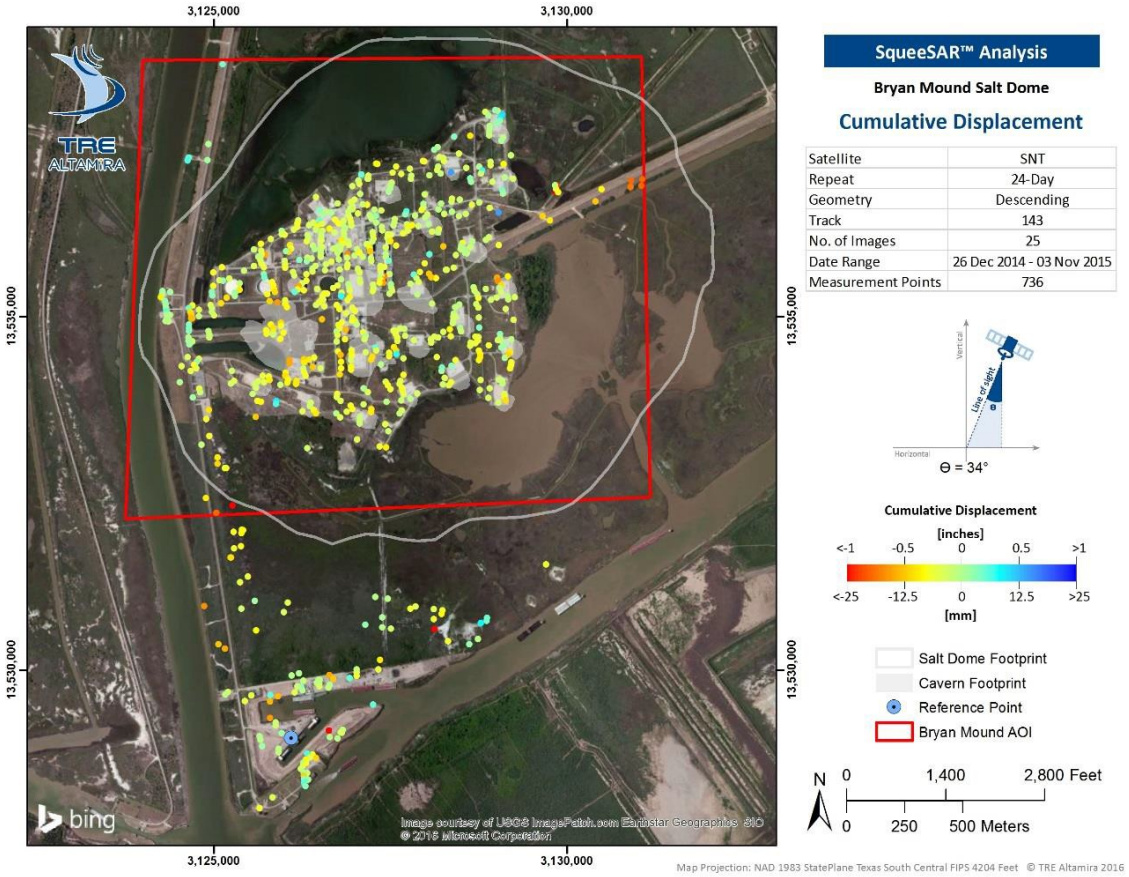

Figure 6: Cumulative displacement obtained from the SNT analysis.

3.2. Displacement Rate

The line-of-sight (LOS) displacement rates detected from the 8-day CSK data set can be seen in the image below (Figure 7). Average annual displacement values are calculated from a linear regression of the ground movement measured over the entire time period covered by the satellite images.

This analysis identified mild deformation over most of the salt dome, with one area of stronger movement observed near storage cavern 3 (up to -0.7 inches/year, or -18.4 mm/year). The average displacement rate across the AOI identified from this analysis is -0.1 inches/year (-3.3 mm/year) which is consistent with subsidence rates previously reported by Sandia National Laboratories via ground surveys (-0.1 inches/year or -3.1 mm/year).

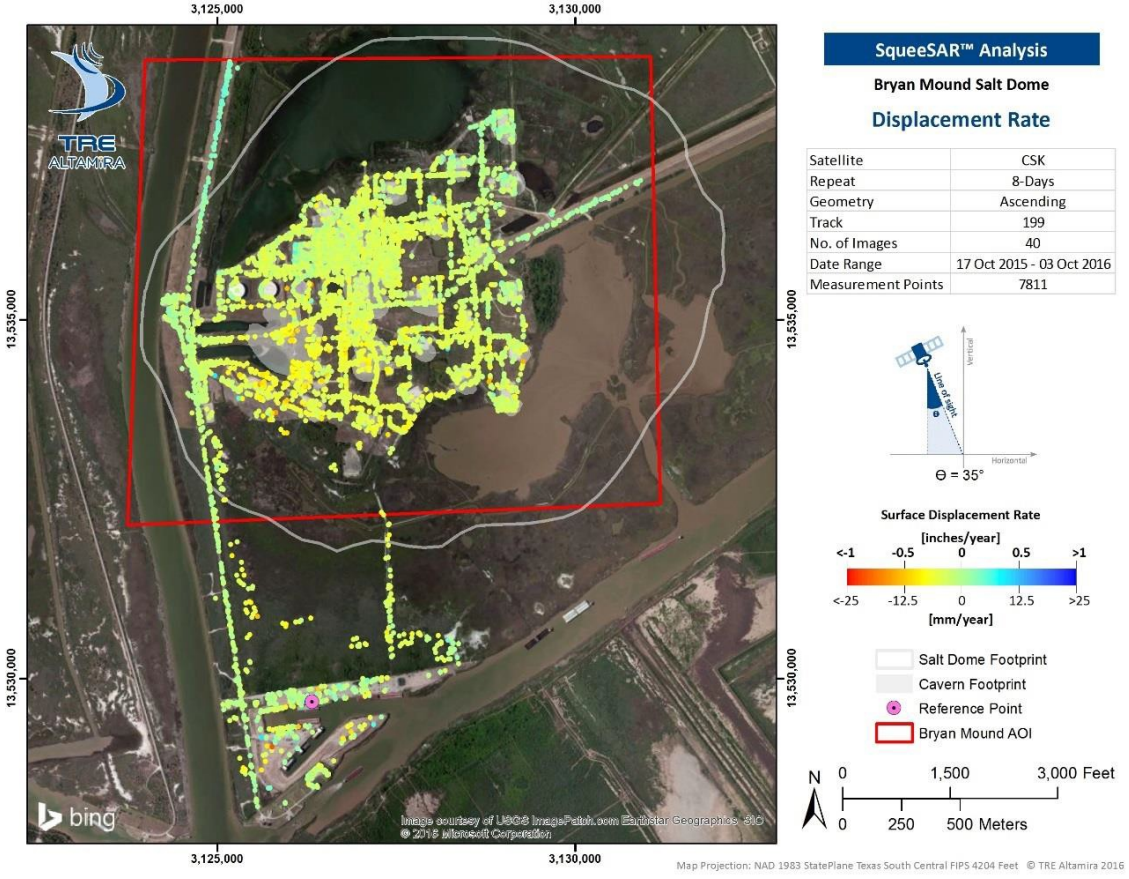

Figure 7: Annual surface displacement rates obtained from the CSK 8-day analysis.

The 16-day CSK analysis identified deformation trends that were largely consistent with the 8-day CSK analysis (Figure 8). Higher deformation rates were again identified near storage cavern 3 (up to -0.8 mm/year, or -21.0 mm/year). The average displacement rate across the entire AOI was -0.2 inches/year (-5.2 mm/year).

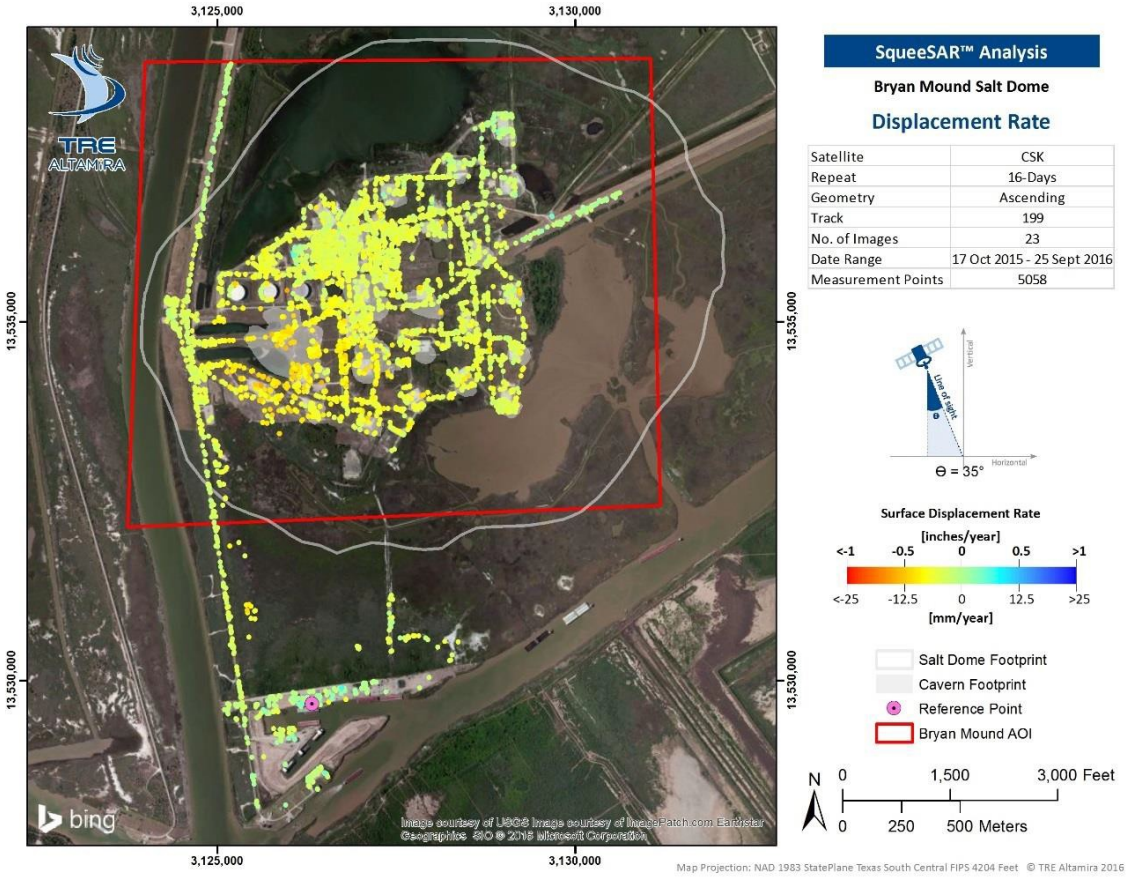

Figure 8: Annual surface displacement rates obtained from the CSK 16-day analysis.

Comparison of surface displacement rate results obtained from the 8- and 16-day CSK SqueeSAR analyses can be seen in Figure 9. This comparison allows for the visualization of movement trends identified over the same time period using different acquisition frequencies. Similar to the cumulative deformation results, annual surface displacement trends appear to be consistent between results obtained from the two repeat frequencies, with slightly higher rates of deformation observed from the 16-day results.

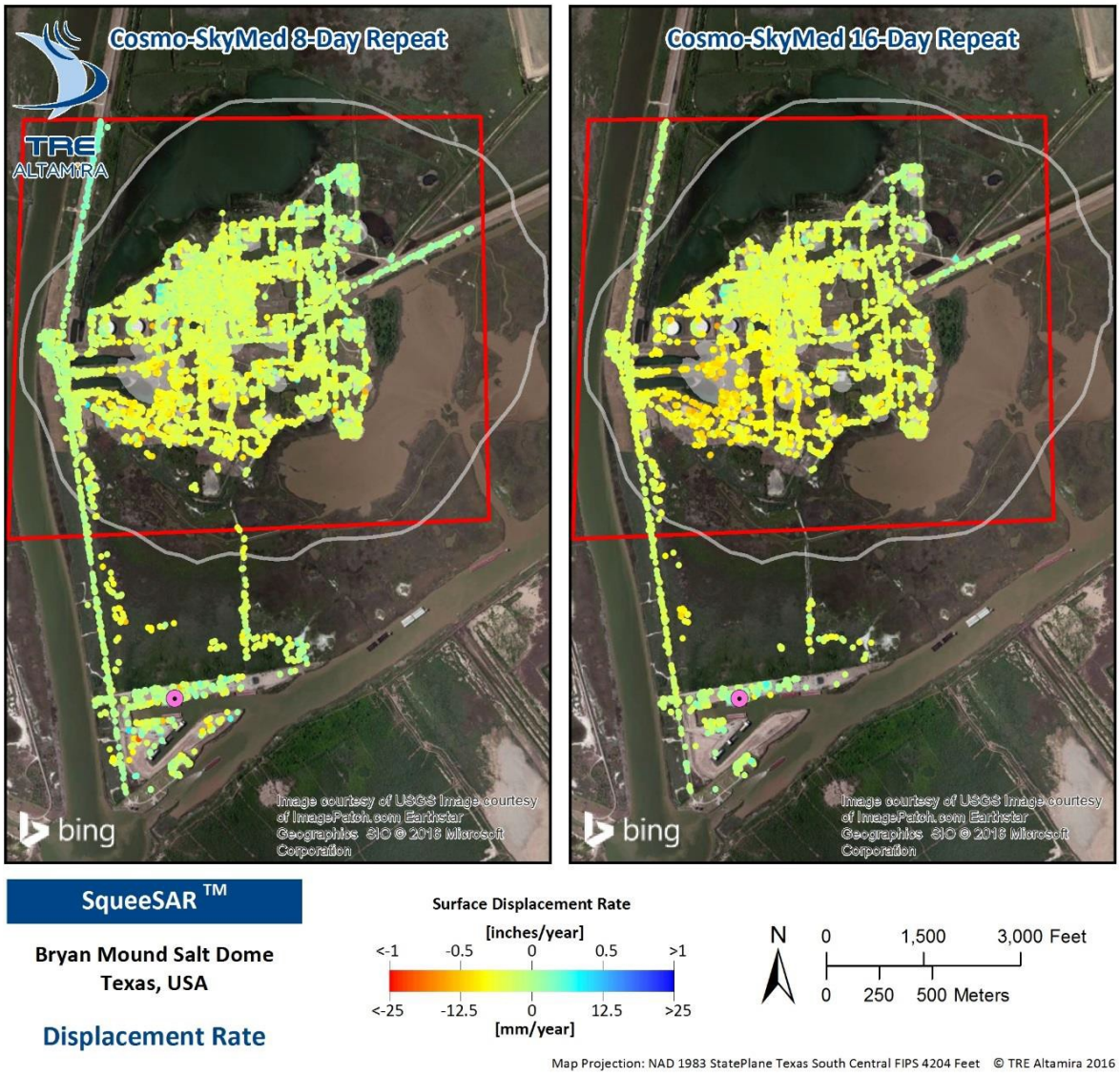

Figure 9: Comparison of annual displacement rates between the CSK analyses.

As seen in Figure 10, the SNT analysis identified subsidence across most of the AOI with an average annual displacement rate of -0.2 inches/year (-5.6 mm/year). Higher rates of subsidence can be observed in the area surrounding cavern 3 and the storage tanks to the north of cavern 3.

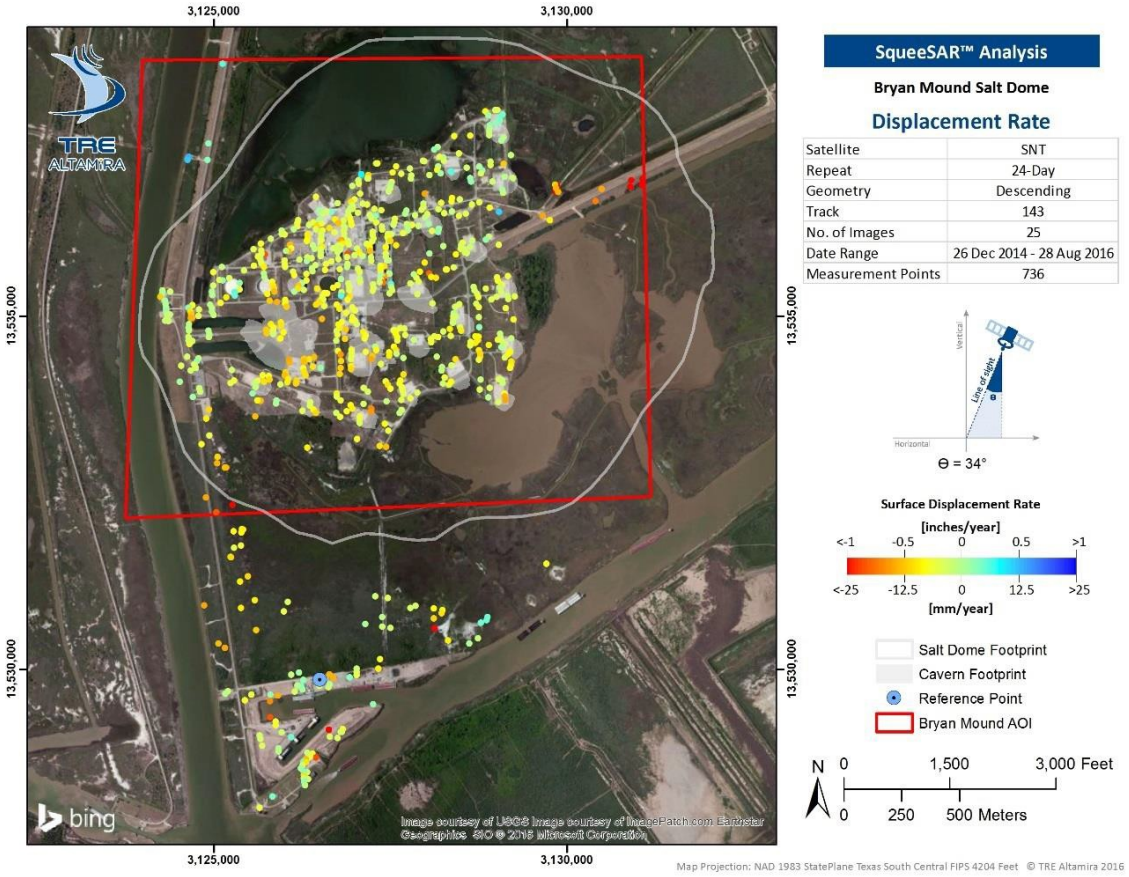

Figure 10: Annual surface displacement rates obtained from the SNT analysis.

3.3. Displacement Rate Standard Deviation

The standard deviation of the surface displacement data characterizes the error associated with the measurements of surface displacement (Figure 11). The displacement rate for a given point should be read as Displacement Rate ± Standard Deviation. Areas impacted by higher standard deviations, indicate a higher variability in measured displacement and are helpful in identifying surface features with rapid or inconsistent movement patterns.

Standard deviation values of the 8-day CSK analysis are low throughout the AOI, with an average standard deviation of ±0.07 inches/year^2 (±1.7 mm/year^2).

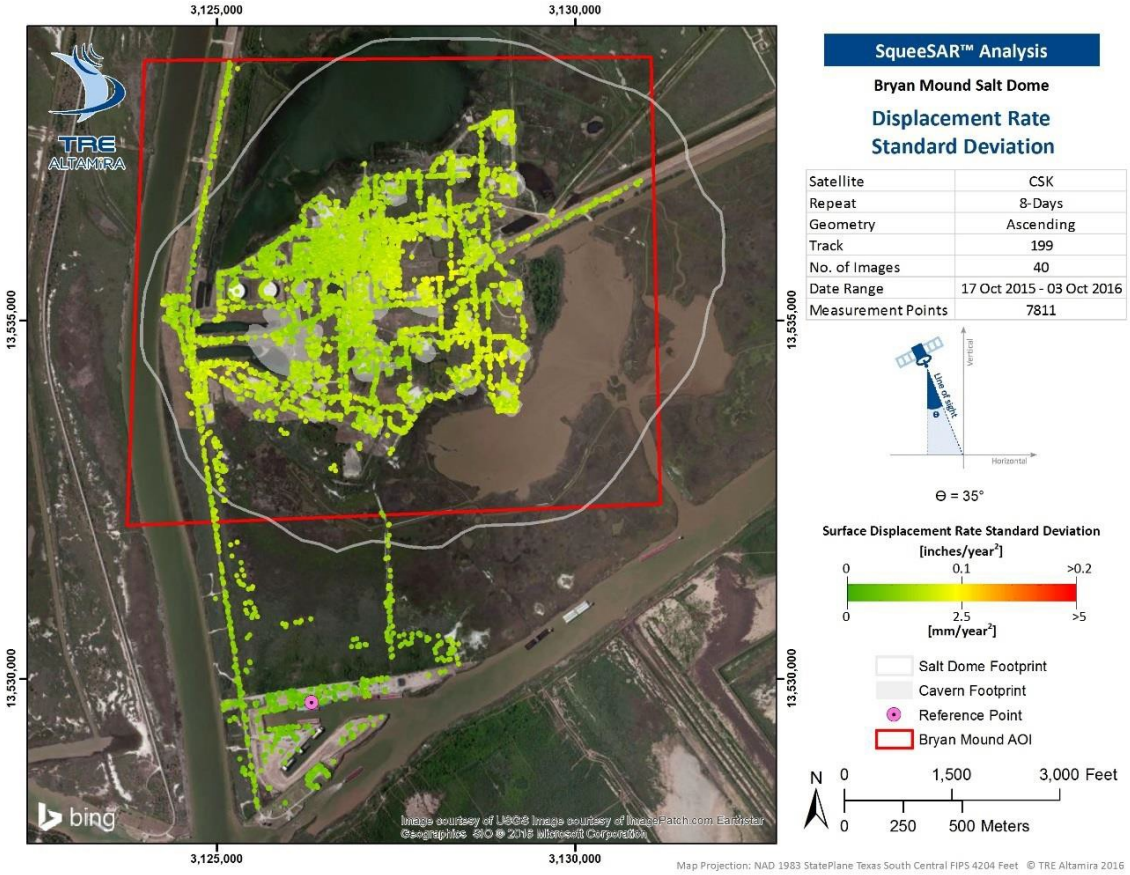

Figure 11: Standard deviation of the annual surface displacement obtained from the CSK 8-day analysis.

Consistent with the 8-day analysis (below), the 16-day CSK analysis results show low standard deviation values across the AOI, with an average standard deviation of ±0.06 inches/year^2 (±1.4 mm/year^2).

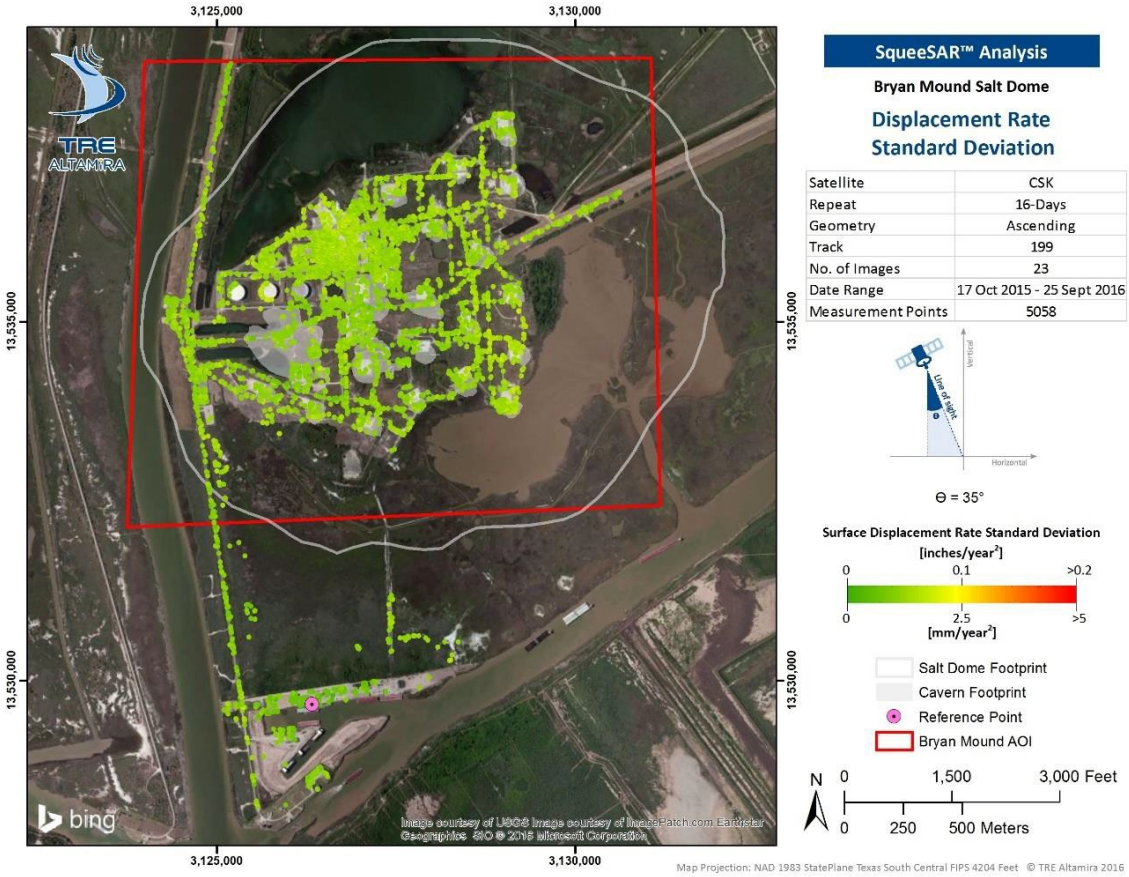

Figure 12: Standard deviation of the annual surface displacement rates obtained from the CSK 16-day analysis.

The standard deviation values of surface displacement identified from the SNT analysis can be seen below in Figure 13. Moderate standard deviation values can be seen across most of the Bryan Mound salt dome with higher values in the north-eastern corner of the AOI. The average standard deviation value is ±0.1 inches/year^2 (±2.8 mm/year^2).

The standard deviation values observed in the results of the SNT SqueeSAR are higher than those identified within the CSK analyses. The precision of displacement rate values depends on various parameters that include the sensor wavelength, the spatial density of measurement points, the distance from the reference point and local ground movement dynamics. The longer wavelength (5.6 cm) of the SNT satellite is also a likely contributor towards the slightly higher standard deviation values.

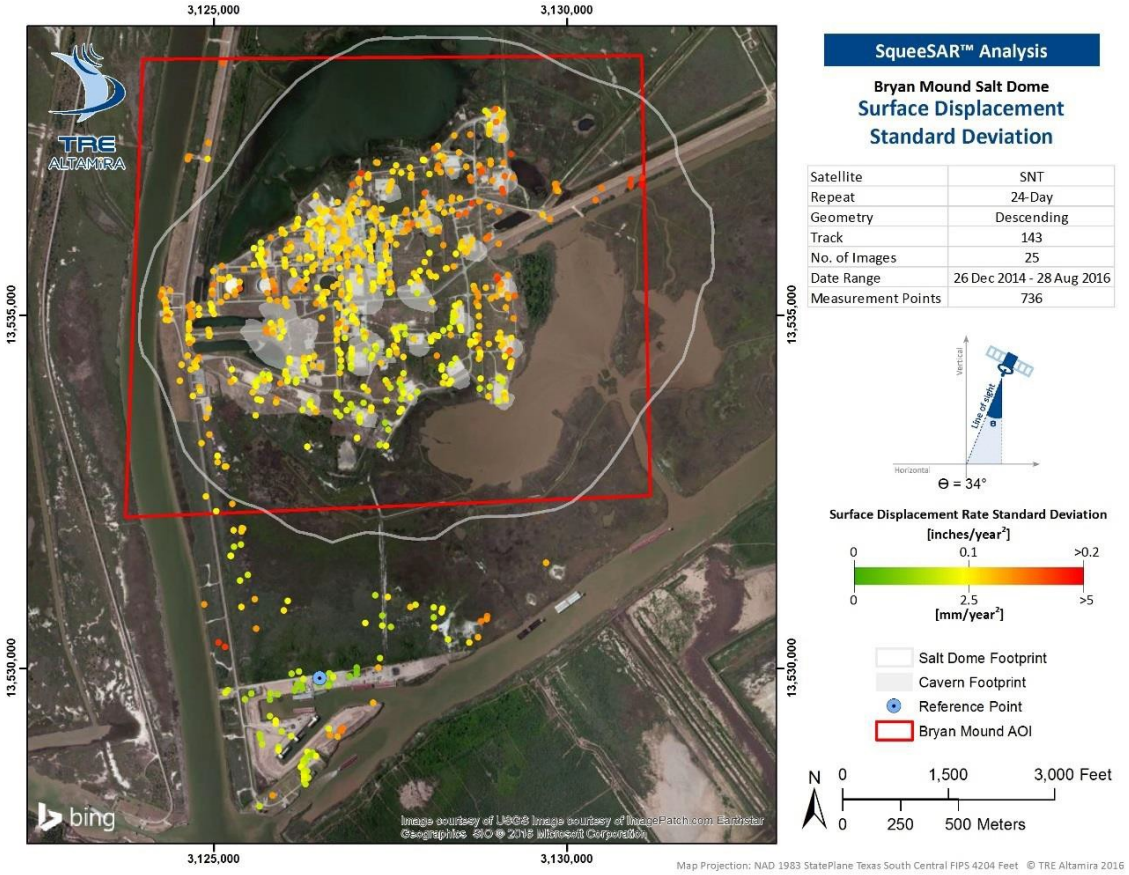

Figure 13: Standard deviation of the annual surface displacement rates obtained from the SNT analysis.

3.4. Acceleration

Acceleration rates of PS and DS can be used to identify non-linear trends in the deformation time series, as well as areas where the deformation rate is increasing or decreasing over time. Negative accelerations, marked in red indicate either an increase in downward movement rates or a decrease in uplift. Positive accelerations, marked in blue, indicate either an increase in upward movement rates, or a decrease in subsidence.

Acceleration values obtained from the 8-day CSK analysis can be seen below in Figure 14. Negative accelerations (up to -1.6 inches/year^2, or -41.3 mm/year^2) were identified across most of the AOI, particularly in the areas surrounding cavern 3 and the storage tanks located north of cavern 3. These acceleration trends indicate an increase in the rate of subsidence identified over these areas. The average acceleration value of all points within the AOI was found to be -0.07 inches/year^2 (-1.9 mm/year^2).

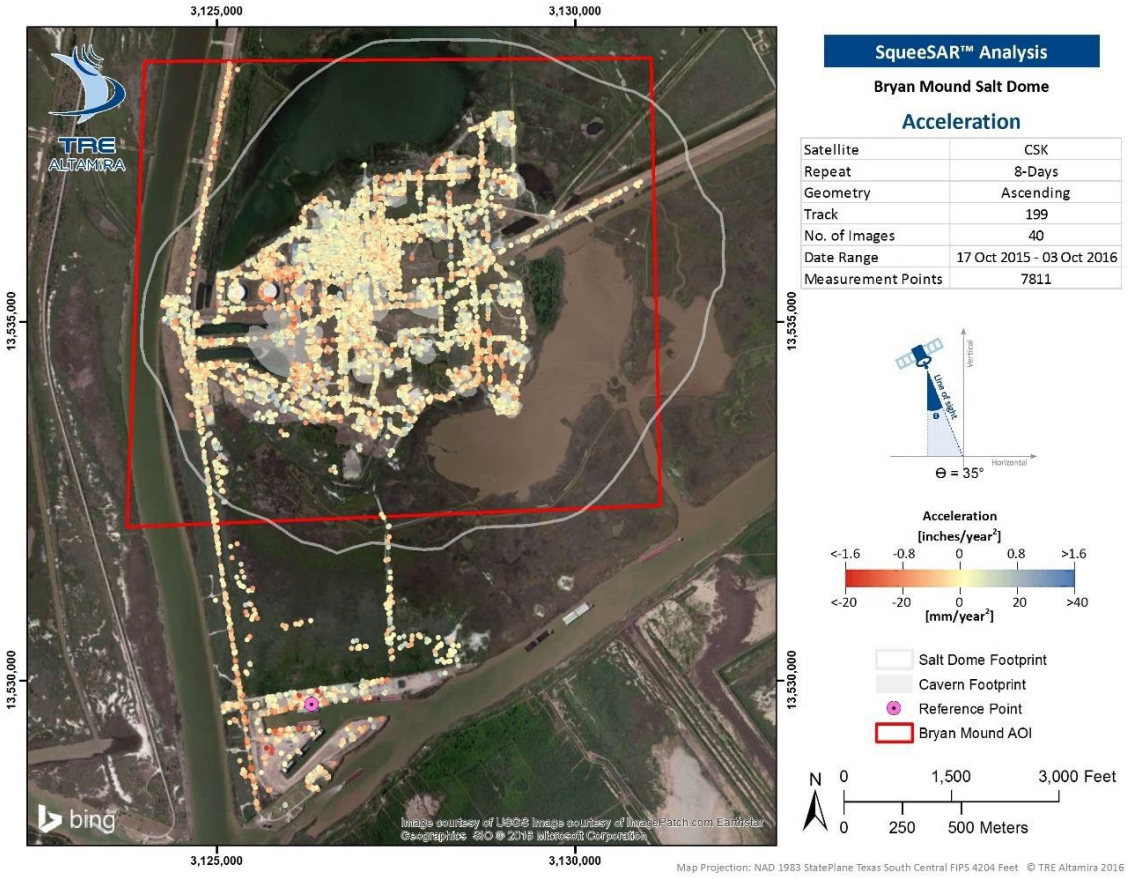

Figure 14: Acceleration rates of the measurement points obtained from the CSK 8-day analysis.

As seen below, acceleration values of the 16-day CSK analysis are mild across most of the AOI (Figure 15). Similar to the results of the 8-day CSK analysis, negative acceleration values (up to -1.2 inches/year^2, or -31.2 mm/year^2) were observed around cavern 3 and storage tanks to the north, indicating an increase in the rate of subsidence. The average acceleration value obtained from all points identified within the AOI was -0.04 inches/year^2 (-1.0 mm/year^2).

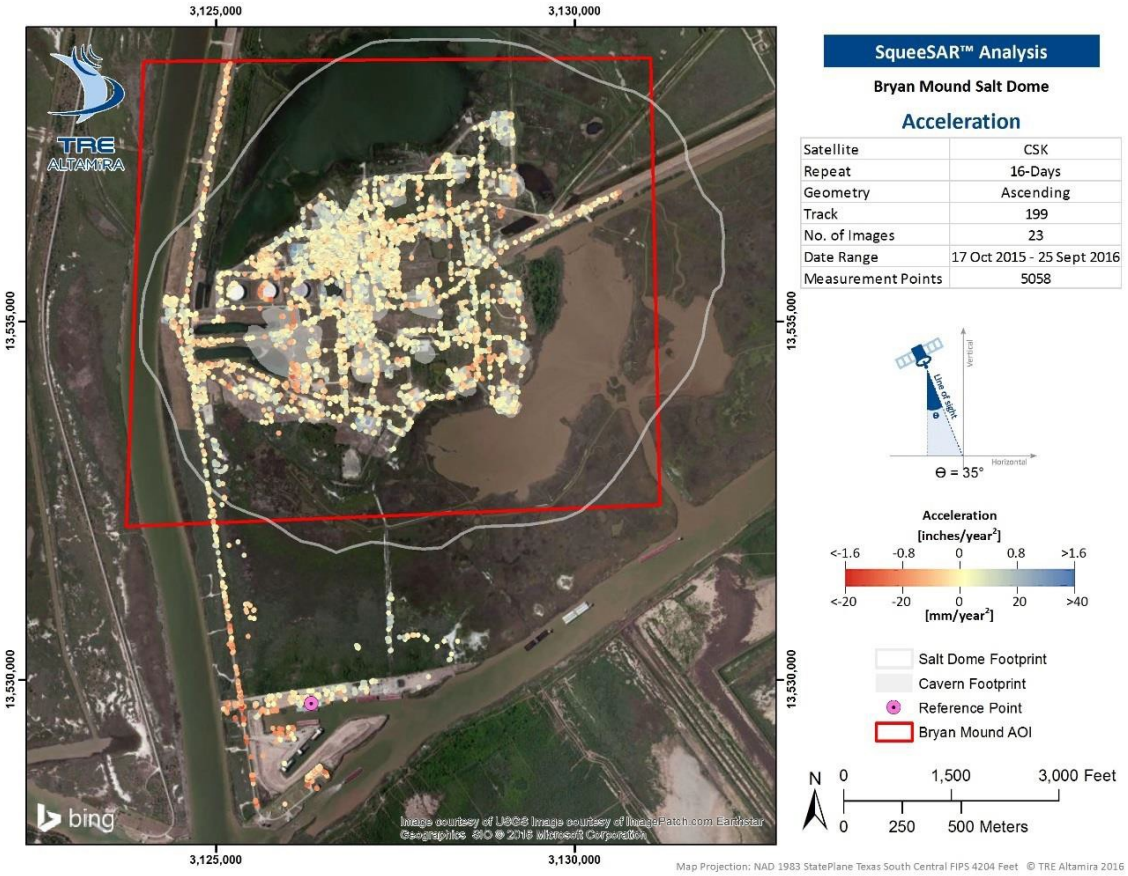

Figure 15: Acceleration rates of measurement points obtained from the CSK 16-Day analysis.

The acceleration values identified from the analysis of the SNT data were more variable in comparison to the CSK results. This is most likely due to the lower precision of the results obtained from this data set. In general, negative acceleration values were identified around the storage tanks to the north of cavern 3, as well as areas surrounding caverns 1, 4 and 104 (Figure 16). Acceleration values as strong as -2.8 inches/year^2 (-70.0 mm/year^2) were identified over these areas, indicating an increase in the rate of subsidence. The average acceleration value of all points within the AOI was -0.01 inches/year^2 (-0.3 mm/year^2). The differences in value with the CSK data can also be caused by the different period of coverage of the data sets.

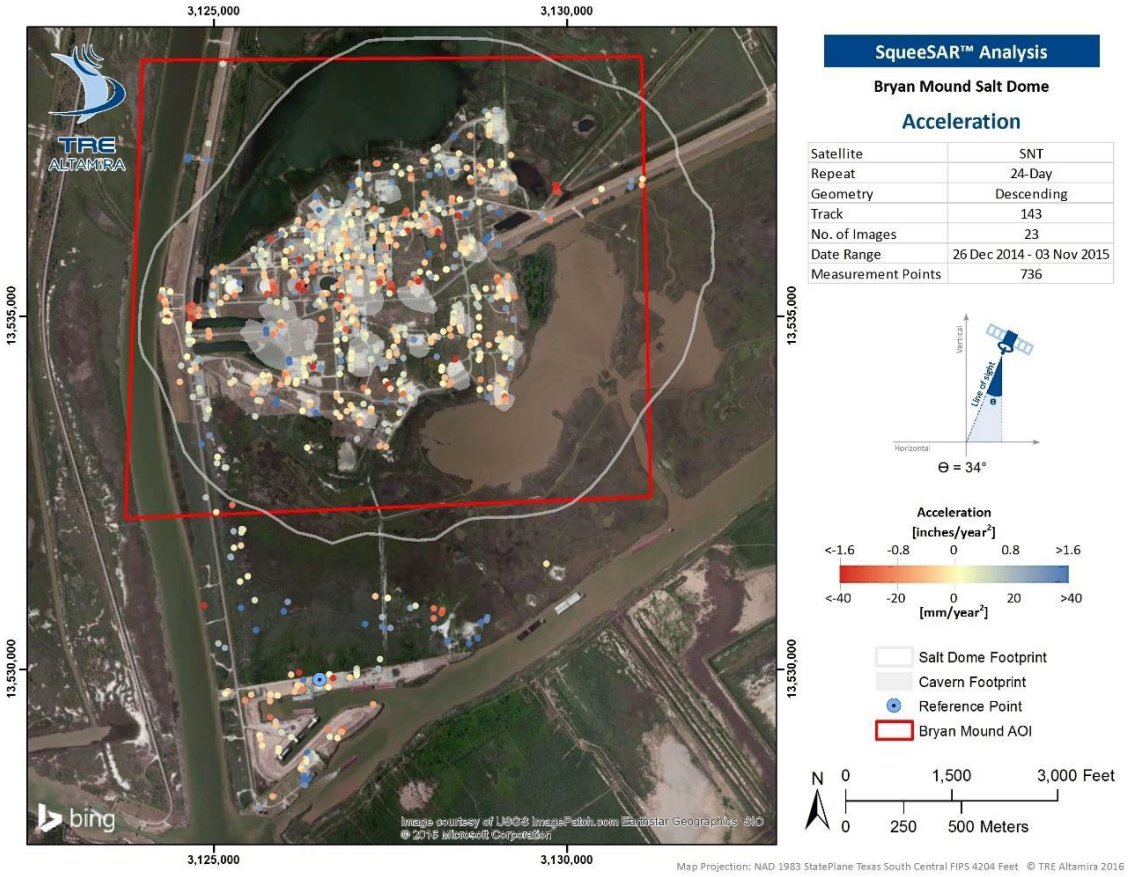

Figure 16: Acceleration rates of the measurement points obtained from the SNT analysis.

4. Observations

4.1. Ground Deformation Over Cavern Footprints

The results of the three SqueeSAR analyses outlined in this report highlight mild subsidence across the surface of the salt dome. Caverns located on the south west portion of the salt dome exhibit higher rates of subsidence in all three data sets. Movement trends were the strongest over cavern 3 for all three analyses. Animations illustrating the evolution of surface deformation over time for each analysis are included as project deliverables.

Six areas of ground movement have been highlighted with average time series (Figure 17). A comparison of the results obtained for each analysis are presented in the following section.

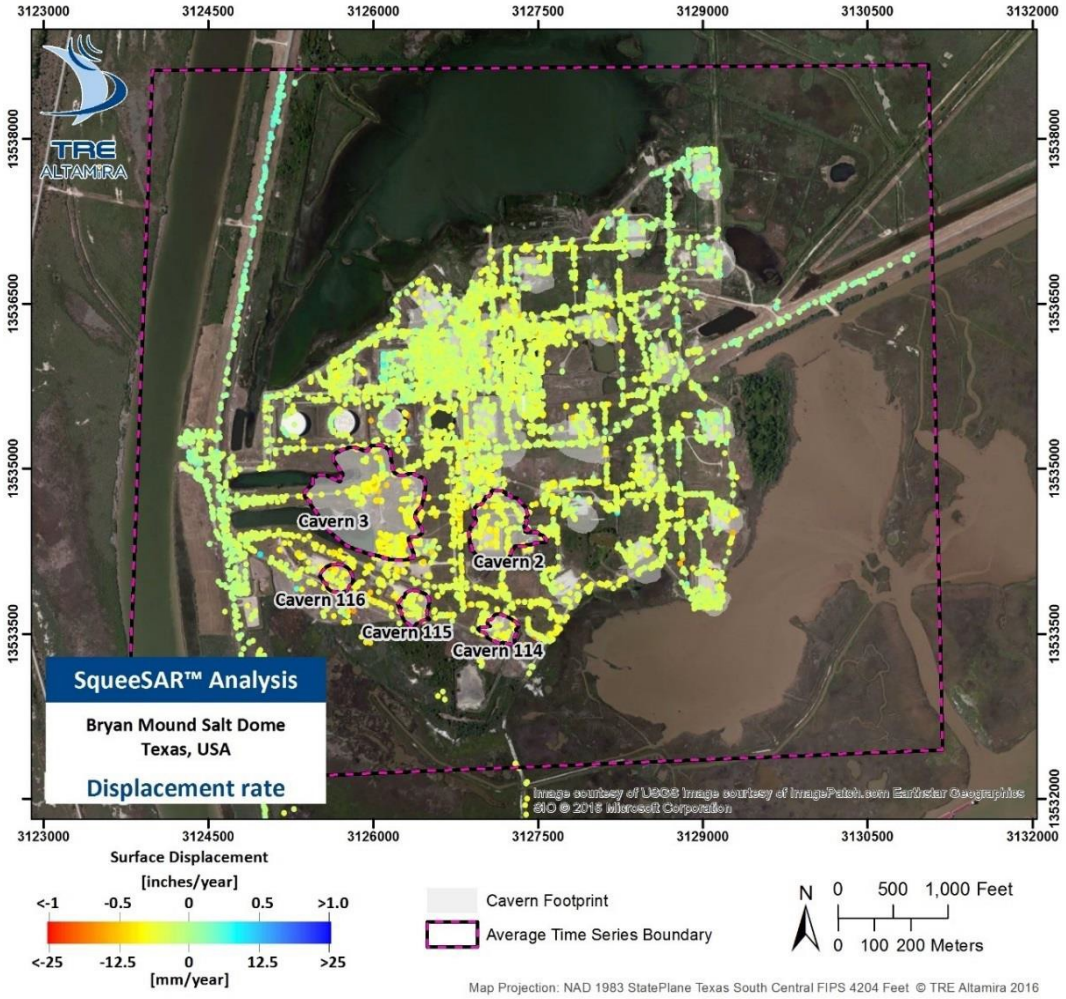

Figure 17: Surface displacement results obtained from the CSK 8-day analysis. Six areas are highlighted and average time series for these features for each data set are shown below in Figure 18 to Figure 35.

4.1.1. Cavern 2 Average Time Series

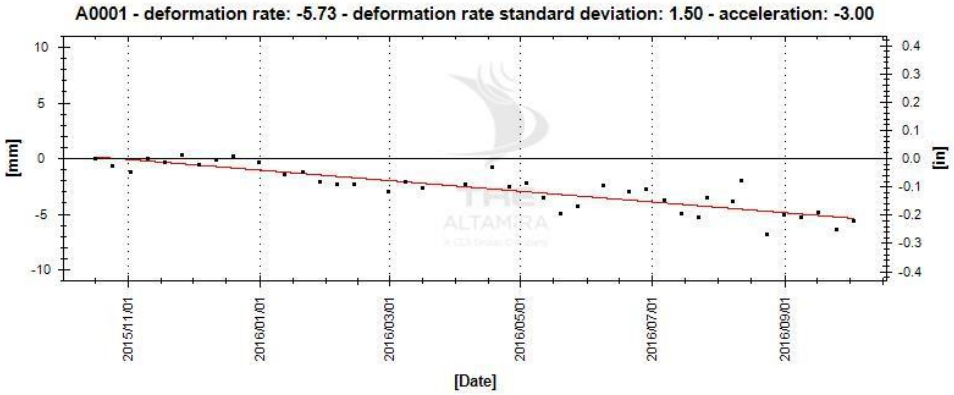

Figure 18: Average time series for all measurement points identified within Cavern 2 (Figure 17) in the CSK 8-day analysis.

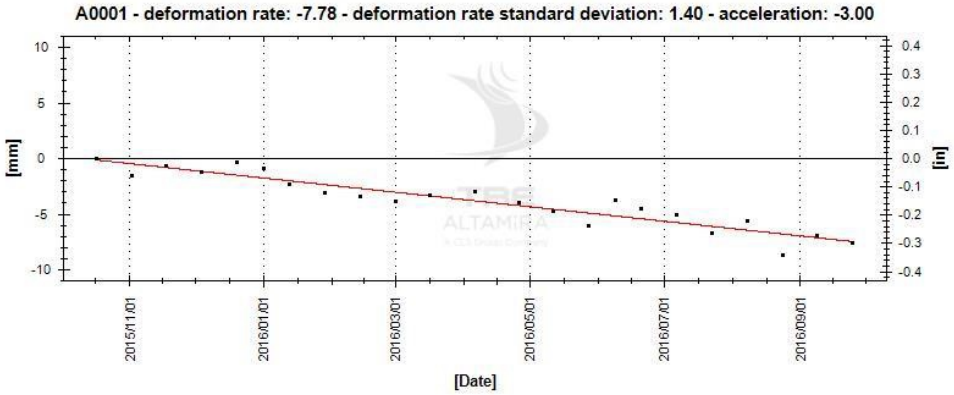

Figure 19: Average time series for all measurement points identified within Cavern 2 (Figure 17) in the CSK 16-day analysis.

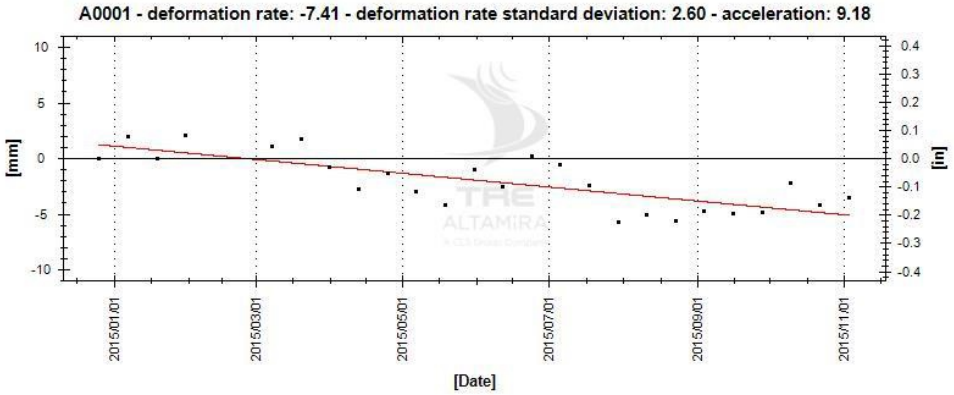

Figure 20: Average time series for all measurement points identified within Cavern 2 (Figure 17) in the SNT analysis.

4.1.2. Cavern 3 Average Time Series

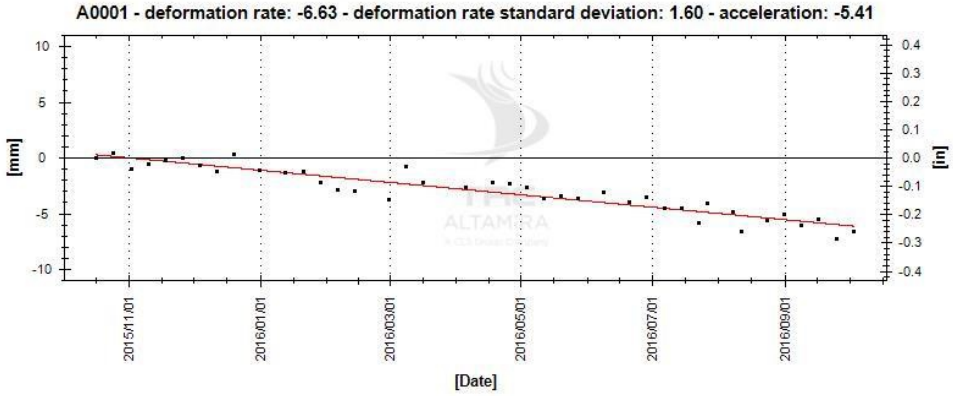

Figure 21: Average time series for all measurement points identified within Cavern 3 (Figure 17) in the CSK 8-day analysis.

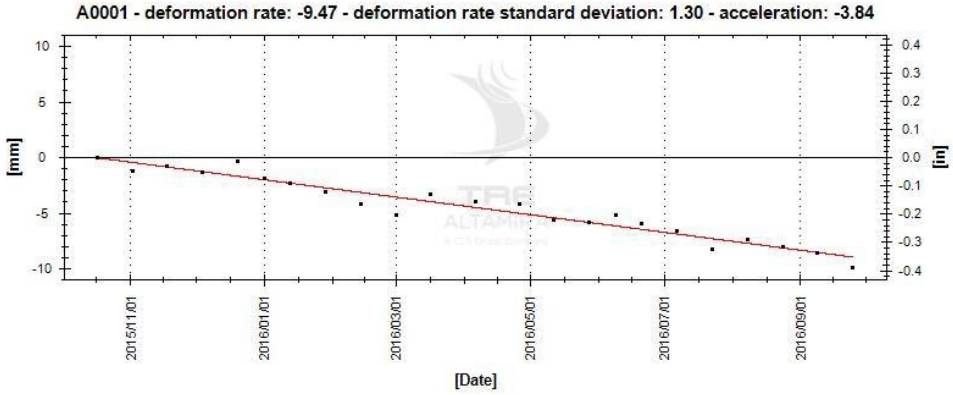

Figure 22: Average time series for all measurement points identified within Cavern 3 (Figure 17) in the CSK 16-day analysis.

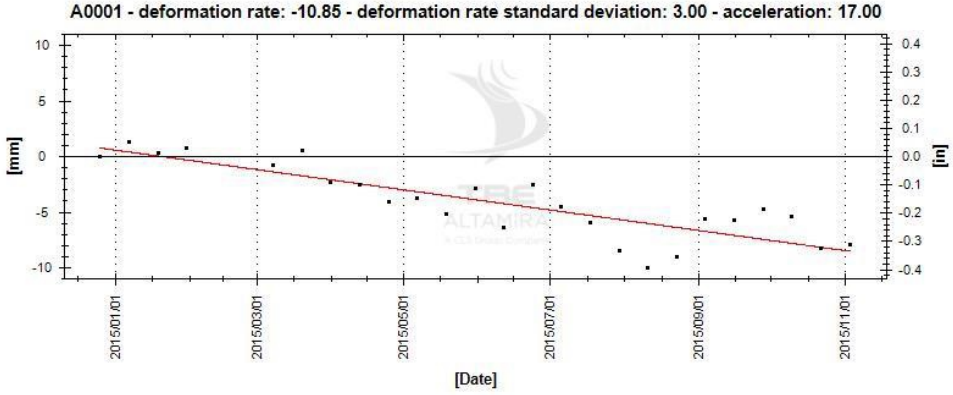

Figure 23: Average time series for all measurement points identified within Cavern 3 (Figure 17) in the SNT analysis.

4.1.3. Cavern 114 Average Time Series

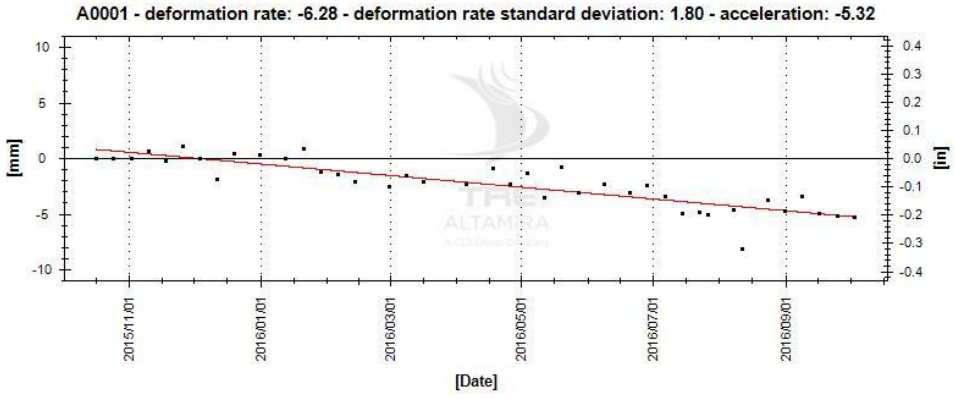

Figure 24: Average time series for all measurement points identified within Cavern 114 (Figure 17) in the CSK 8-day analysis.

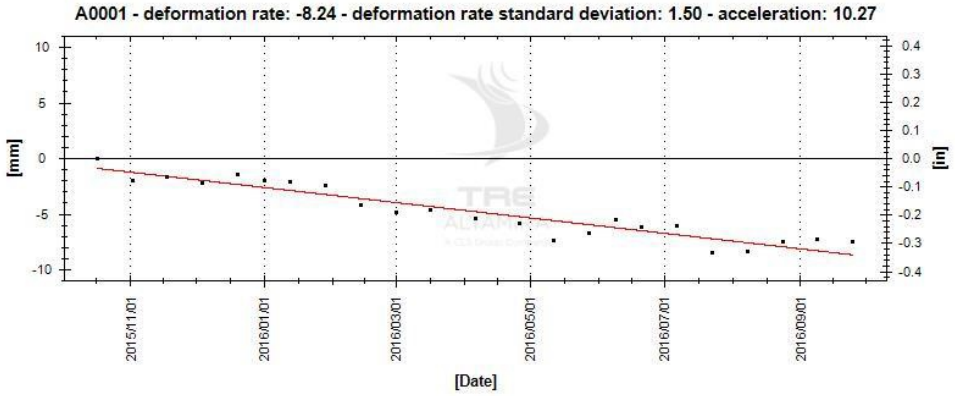

Figure 25: Average time series for all measurement points identified within Cavern 114 (Figure 17) in the CSK 16-day analysis.

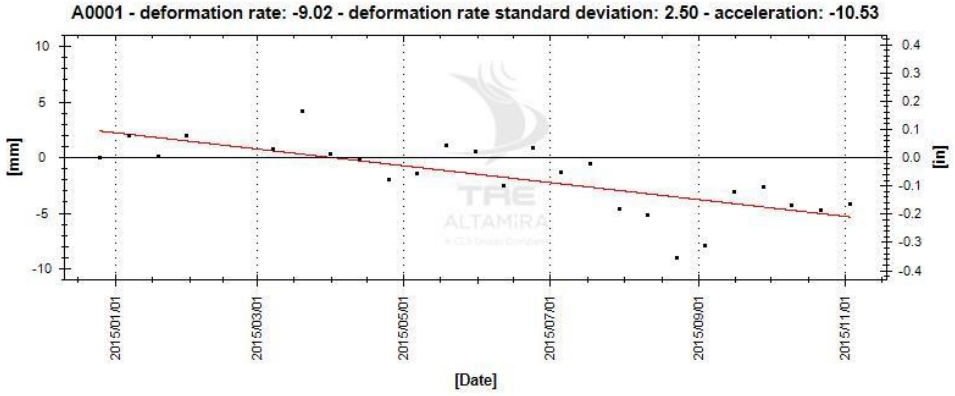

Figure 26: Average time series for all measurement points identified within Cavern 114 (Figure 17) in the SNT analysis.

4.1.4. Cavern 115 Average Time Series

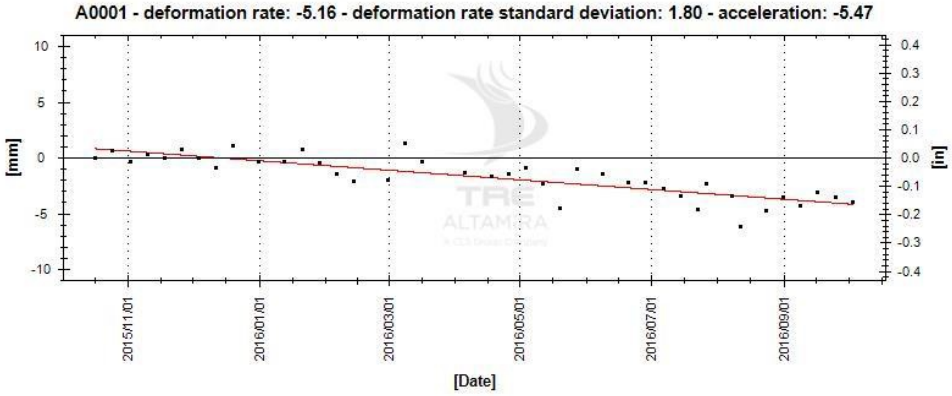

Figure 27: Average time series for all measurement points identified within Cavern 115 (Figure 17) in the CSK 8-day analysis.

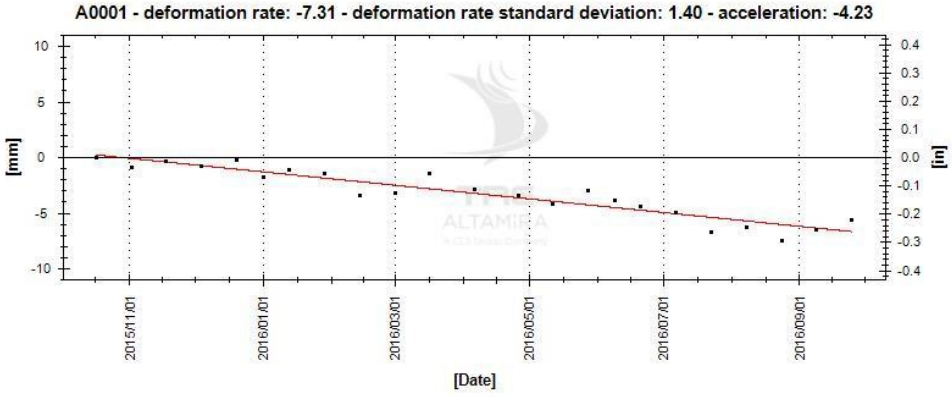

Figure 28: Average time series for all measurement points identified within Cavern 115 (Figure 17) in the CSK 16-day analysis.

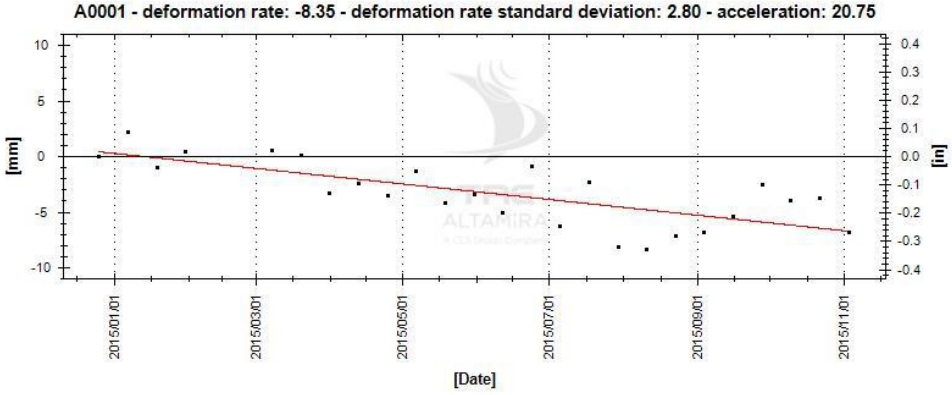

Figure 29: Average time series for all measurement points identified within Cavern 115 (Figure 17) in the SNT analysis.

4.1.5. Cavern 116 Average Time Series

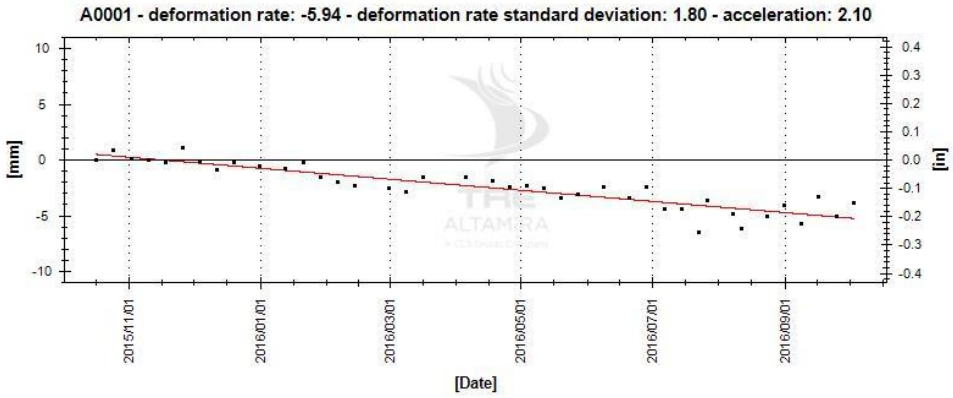

Figure 30: Average time series for all measurement points identified within Cavern 116 (Figure 17) in the CSK 8-day analysis.

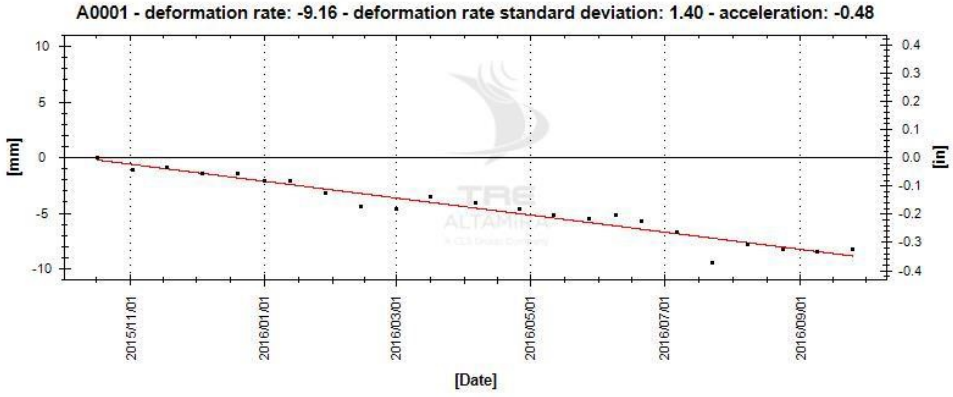

Figure 31: Average time series for all measurement points identified within Cavern 116 (Figure 17) in the CSK 16-day analysis.

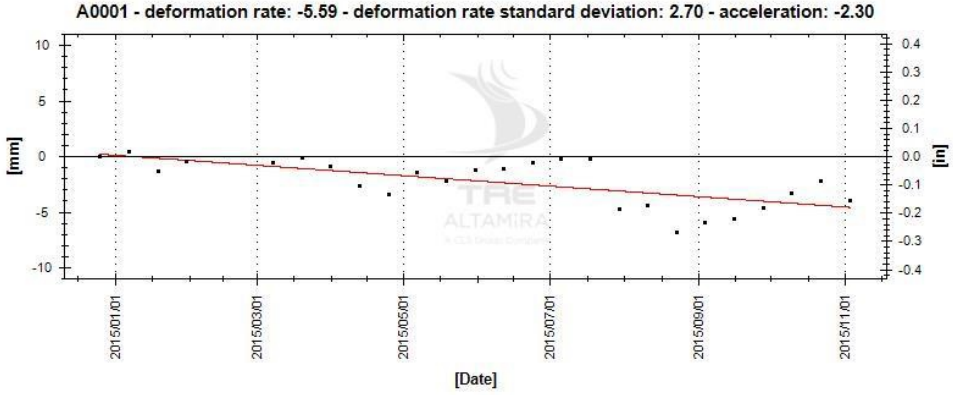

Figure 32: Average time series for all measurement points identified within Cavern 116 (Figure 17) in the SNT analysis.

4.1.6. Full AOI Average Time Series

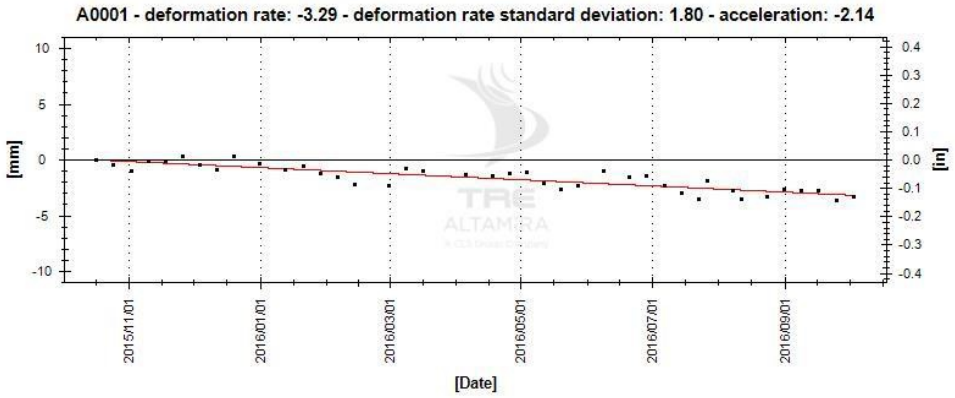

Figure 33: Average time series for all measurement points identified within the AOI (Figure 17) in the CSK 8-day analysis.

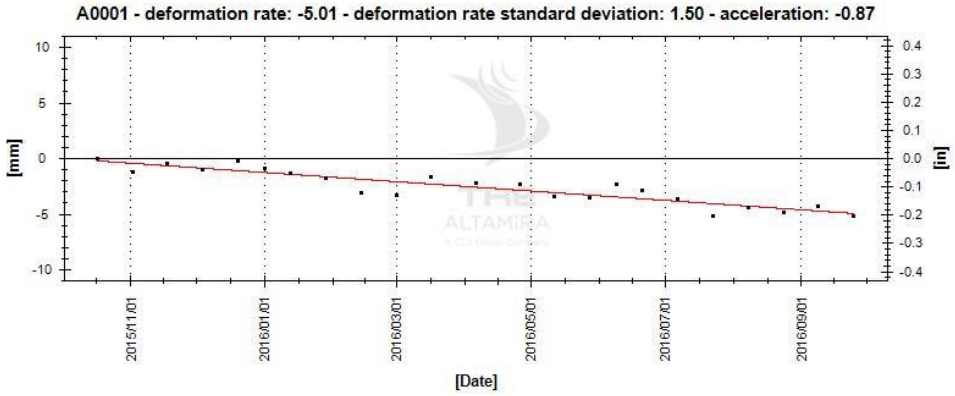

Figure 34:Average time series for all measurement points identified within the AOI (Figure 17) in the CSK 16-day analysis.

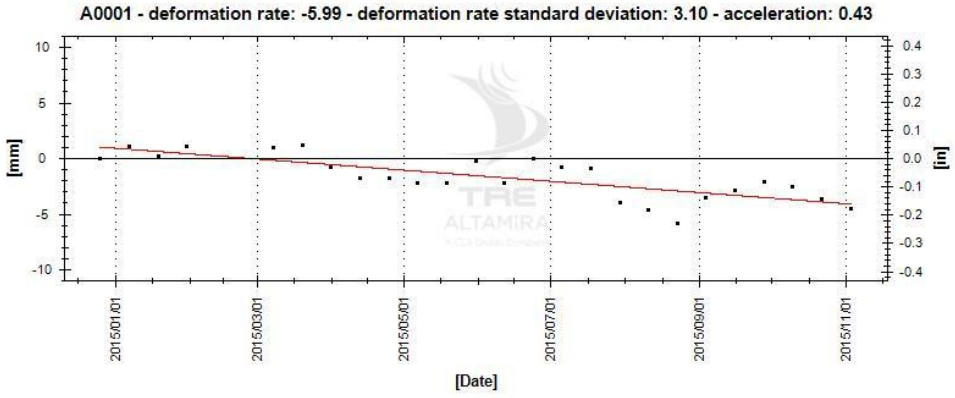

Figure 35: Average time series for all measurement points identified within the AOI (Figure 17) in the SNT analysis.

4.2. SqueeSAR Analyses Comparison

A summary of average deformation values obtained from the average time series shown in Section 4.1 can be seen in Table 5. Rates of subsidence were consistently lowest in the 8-day CSK analysis and highest in the SNT analysis. When comparing the CSK and SNT data sets, differences in the period of coverage and satellite viewing geometry should be considered. As the CSK and SNT image stacks are acquired from ascending and descending orbital geometries, ground deformation is captured from different perspectives. This means slightly different movement patterns can be highlighted in the results.

The precision of the measurements was anticipated to be the slightly higher for the 8-day CSK analysis (compared to the 16-day data) as this data set contained the highest number of images and produced the highest density of measurement points. However, the standard deviation values were slightly lower for the 16-day CSK data set. This is likely due to the short duration of this analysis and the possible presence of one or two lower quality images in this data set compared to the 16-day data set. Standard deviation values are expected to decrease as more images are included in each processing.

		CSK 8-Day	CSK 16-Day	SNT 12-Day
Cavern 2	Deformation Rate (mm/year)	-5.73	-7.78	-7.41
	Deformation Rate Standard Deviation (mm/year²)	±1.50	±1.40	±2.60
Cavern 3	Deformation Rate (mm/year)	-6.63	-9.47	-10.85
	Deformation Rate Standard Deviation (mm/year²)	±1.60	±1.30	±3.00
Cavern 114	Deformation Rate (mm/year)	-6.28	-8.24	-9.02
	Deformation Rate Standard Deviation (mm/year²)	±1.80	±1.50	±2.50
Cavern 115	Deformation Rate (mm/year)	-5.16	-7.31	-8.35
	Deformation Rate Standard Deviation (mm/year²)	±1.80	±1.40	±2.80
Cavern 116	Deformation Rate (mm/year)	-5.94	-9.16	-5.59
	Deformation Rate Standard Deviation (mm/year²)	±1.80	±1.40	±2.70
Full AOI	Deformation Rate (mm/year)	-3.29	-5.01	-5.99
	Deformation Rate Standard Deviation (mm/year²)	±1.80	±1.50	±3.10

Table 5: Deformation measurements obtained from average time series in Figure 18 to Figure 35.

4.3. Ground Deformation Surface Profiles

4.3.1. Cavern 3

A surface profile along the road over cavern 3 was created to illustrate changes in surface deformation patterns over time (Figure 36). A surface profile cross section was generated by averaging all SqueeSAR points within a 100-foot (30.5 meter) buffer of the profile line displayed below. As much as -0.3 inches (-8.4 mm) of subsidence was measured along this profile since October 2015. An animation of ground displacement over cavern 3 has been provided as a deliverable along with this report.

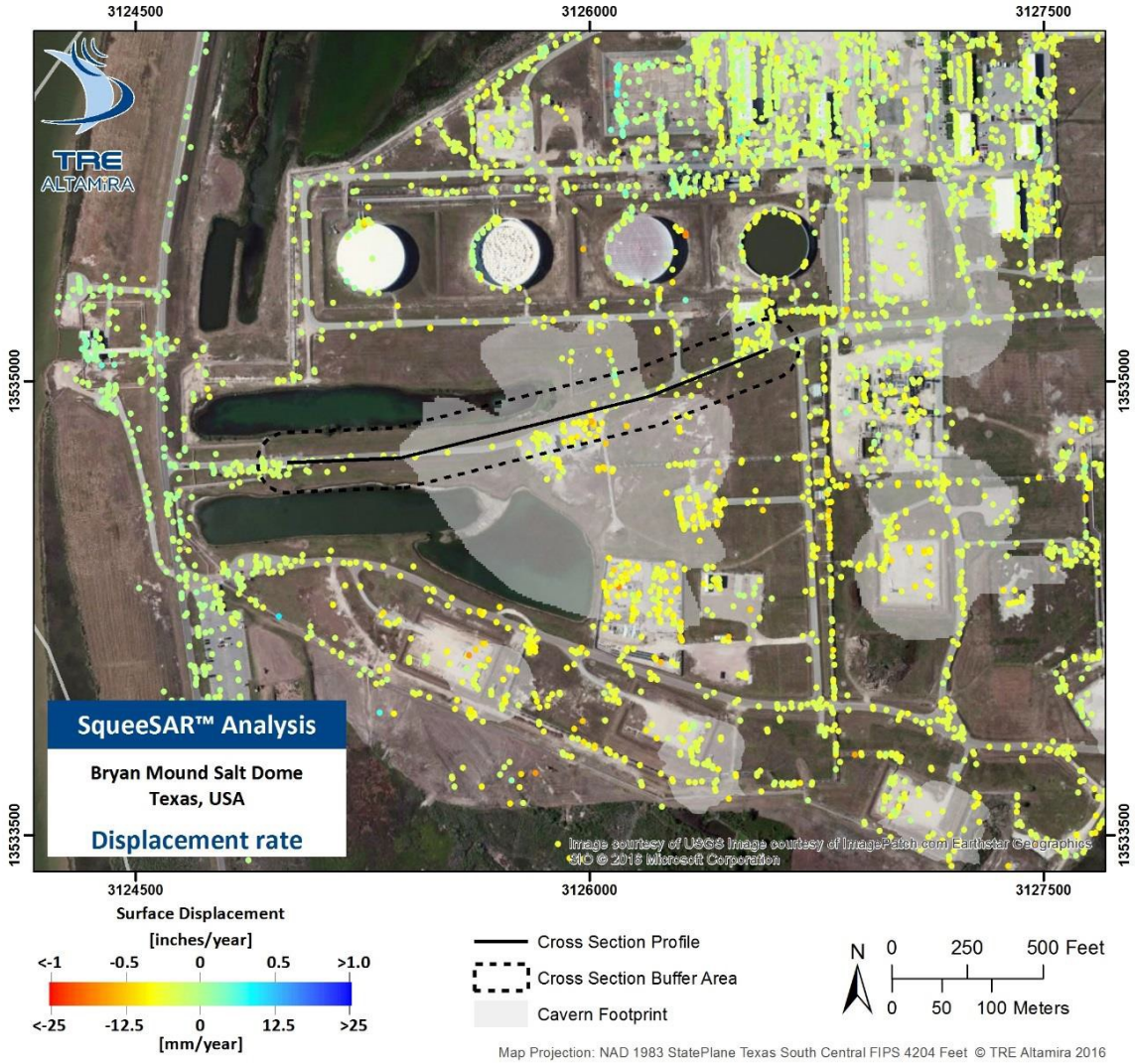

Figure 36: Trace of the surface profile cross-section over Cavern 3. Cross section shown in Figure 37.

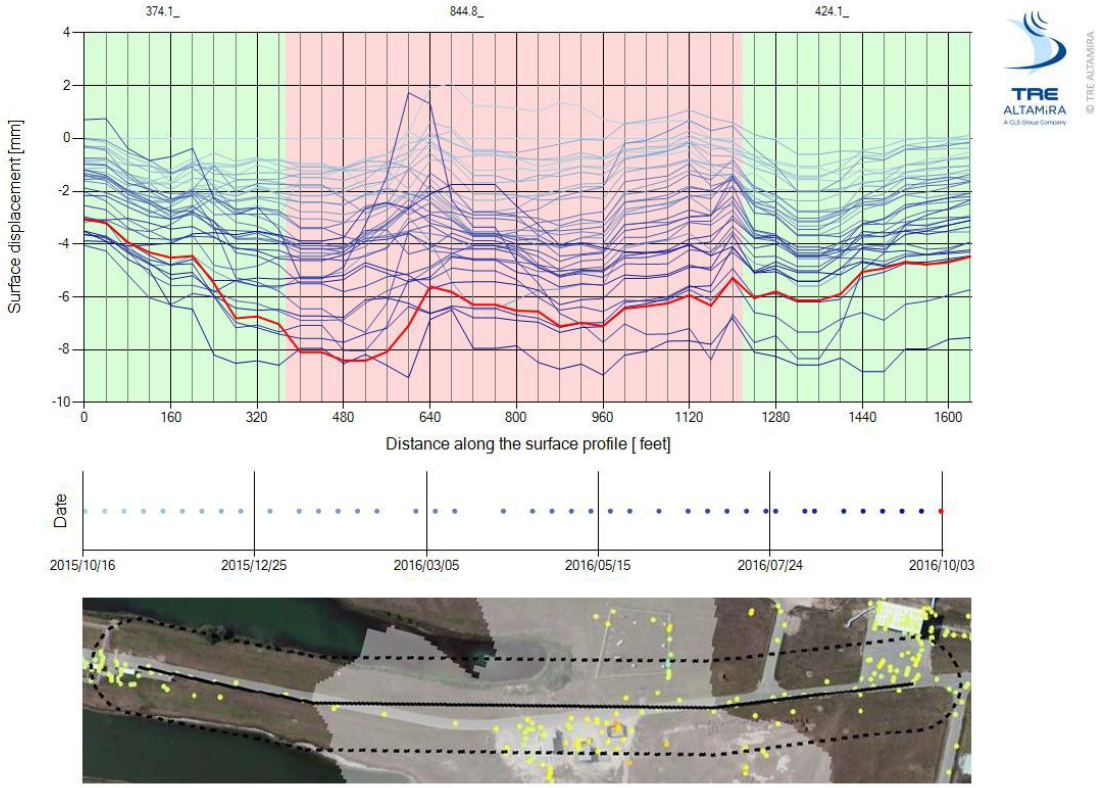

Figure 37: Evolution of the surface profile cross section in Figure 36. The profile highlighted in red corresponds to the final image of the data stack.

4.3.2. Full Salt Dome

A surface profile was created across the entire salt dome to illustrate deformation changes over time, and to highlight subsidence behaviour across the centre of the salt dome. All SqueeSAR points within a 100-foot (34.5 meter) buffer of the central road were averaged. The profile line also crosses through caverns 1, 3 and 4. An animation of ground displacement along this profile has been provided.

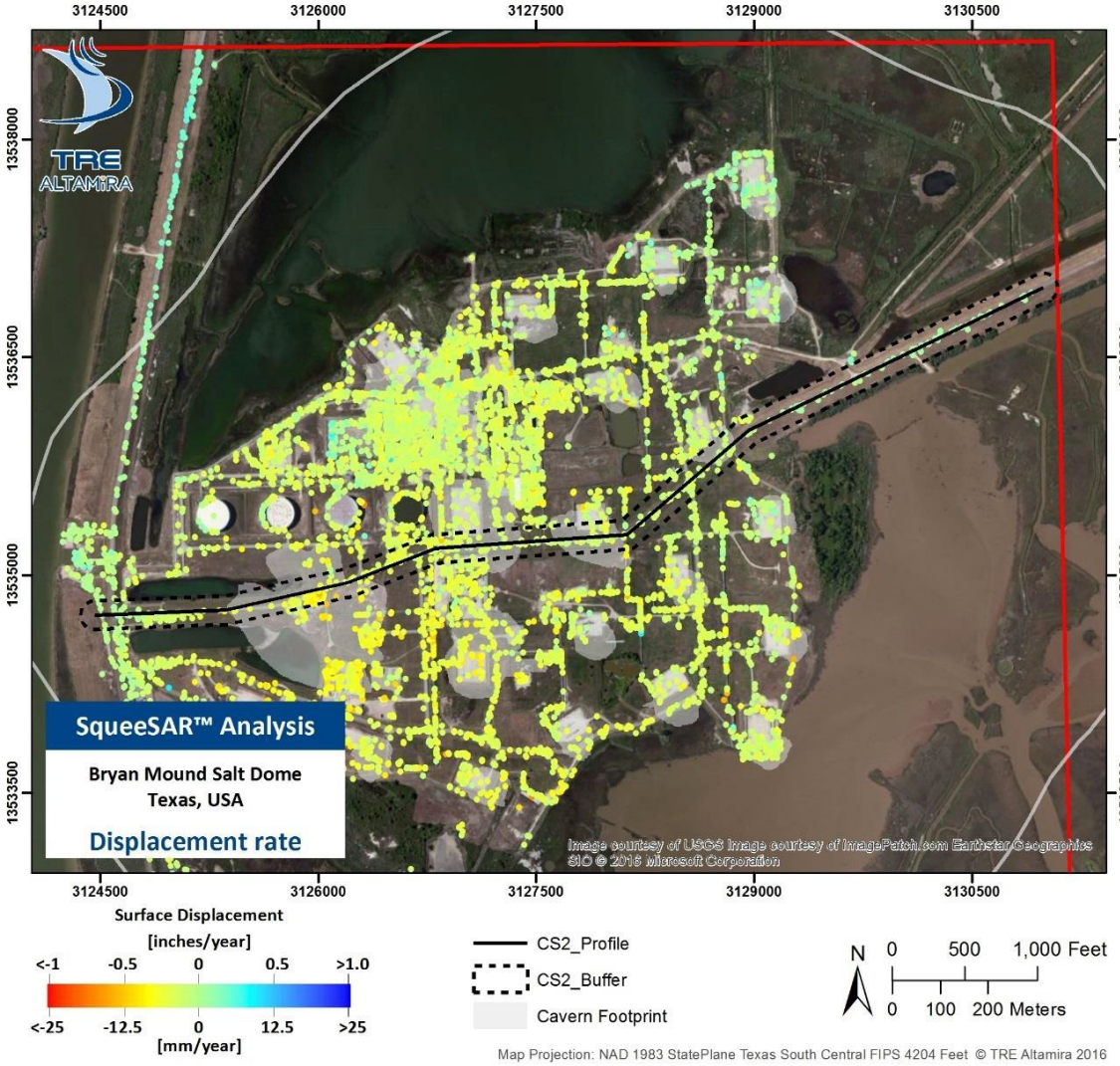

Figure 38: Trace of the surface profile cross-section over the full salt dome, following the main road. Cross section shown in Figure 39.

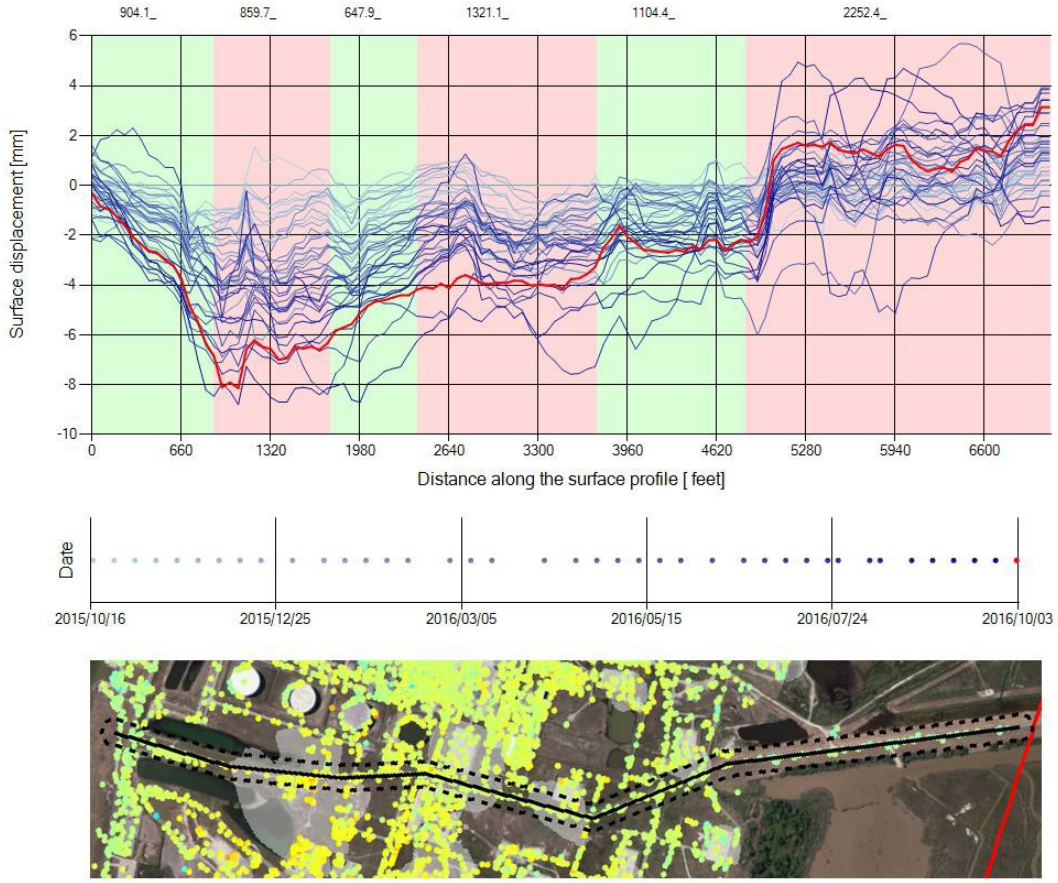

Figure 39: Evolution of the surface profile cross section indicated by Figure 38. The profile highlighted in red corresponds to the final image of the data stack.

4.4. Results over Benchmarks

Comparisons between SqueeSAR results and a network of benchmarks used in ground-based surveying can be made by projecting ground survey data to the line-of-site (LOS) of the satellite. It is possible to convert the vertical measurements to LOS displacement using the following equation, bearing in mind that the underlying assumption is that all displacement measured by the satellite is vertical (e.g. no horizontal component is present).

$$\text{LOS displacement} = \text{vertical displacement} \times \cos(\text{incidence angle})$$

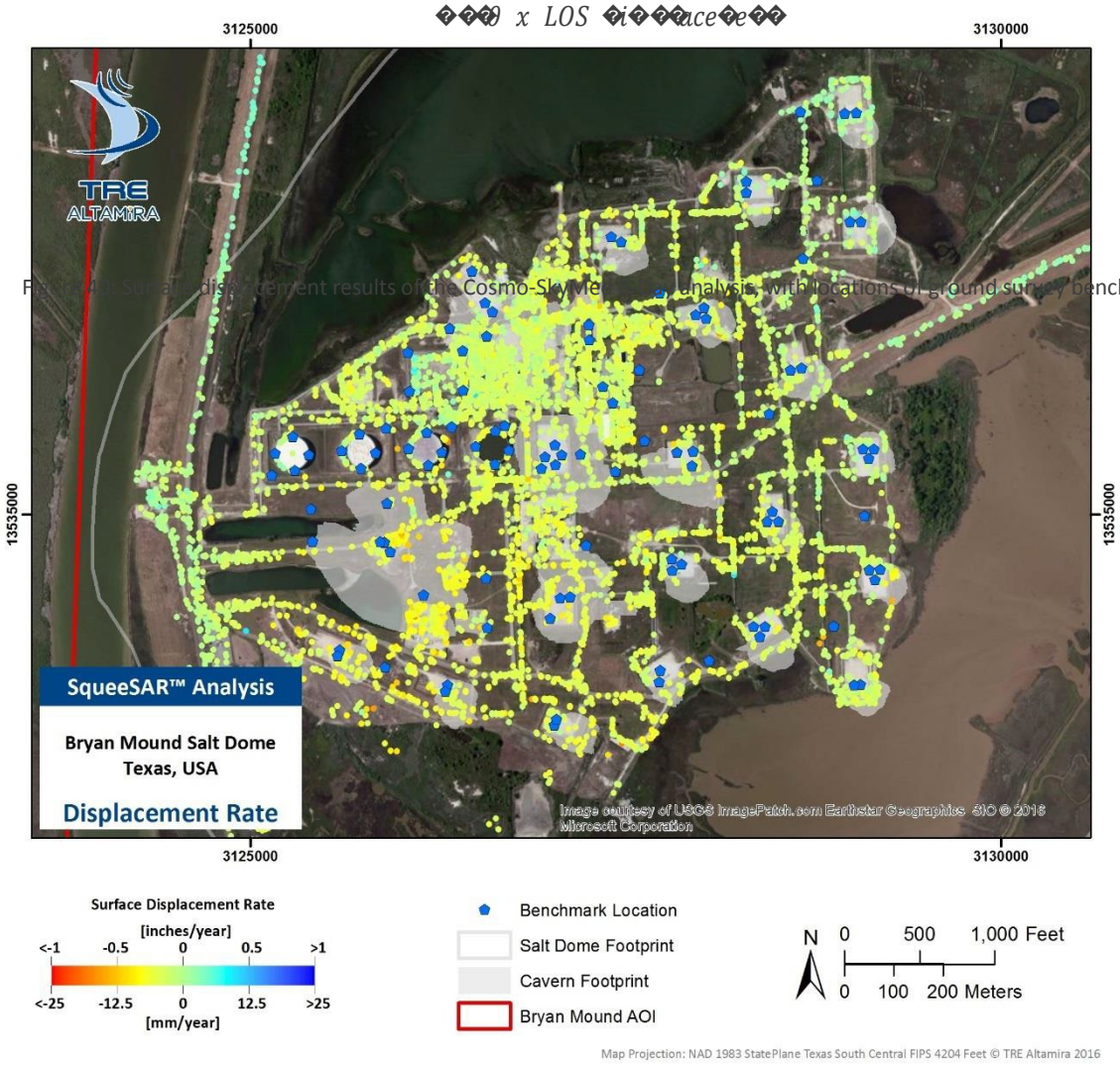

Figure 4-1: Surface displacement results of the Cosmo-SkyMed SqueeSAR analysis, with locations of ground survey benchmarks.

In the figure shown below, survey benchmarks are color-coded according to the SqueeSAR LOS results obtained for each location. SqueeSAR values for each benchmark location were extracted from an interpolation of the CSK 8-day results. Benchmark locations have been approximated with a supervised spatial adjustment procedure applied to an unknown local coordinate system. Comparisons should therefore be undertaken with caution. To help facilitate comparisons between the SqueeSAR data and ground-based survey results, .csv data files containing the deformation measurements identified at all benchmark locations have been provided as deliverables along with this report.

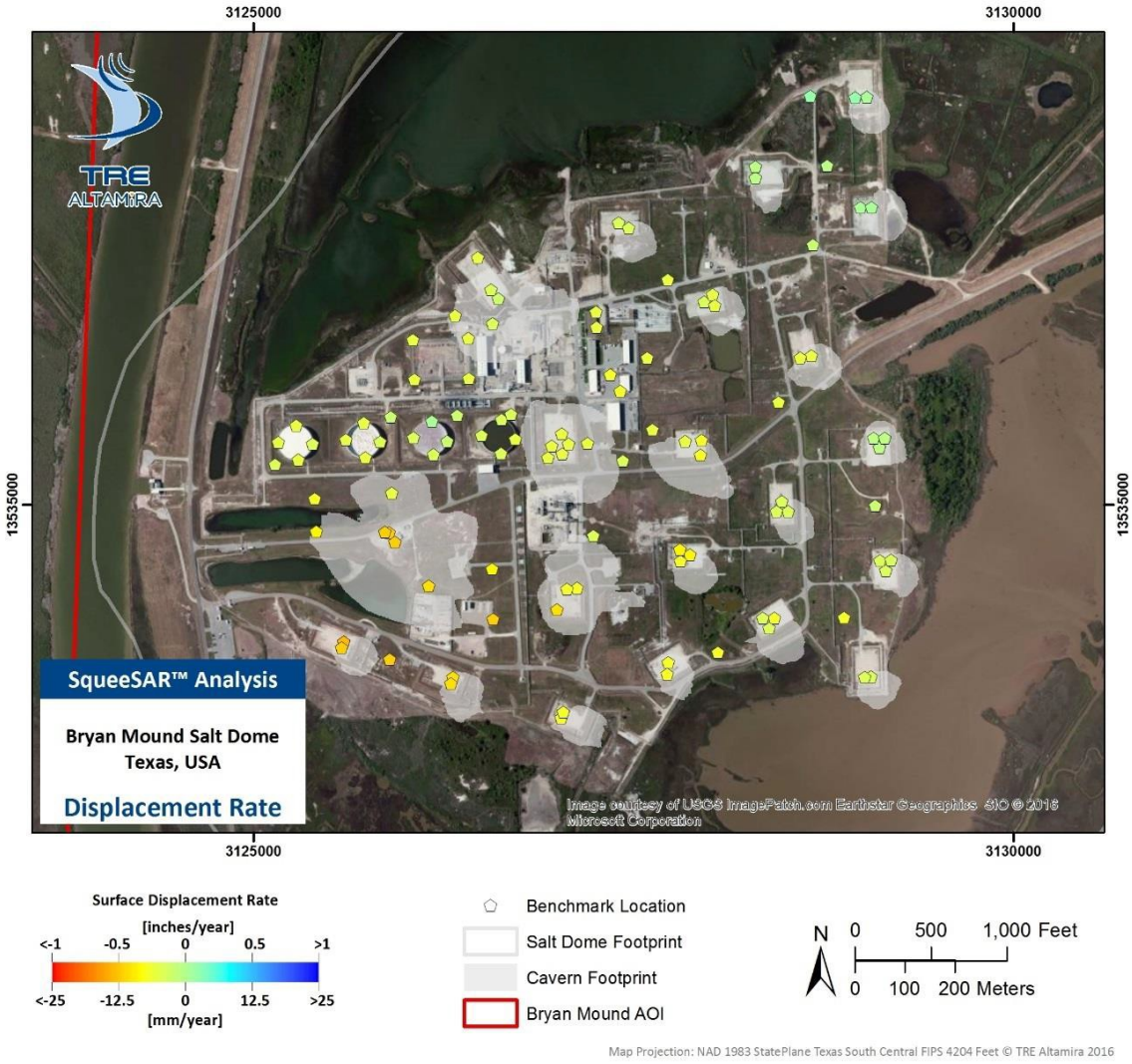

Figure 41: Surface displacement rate results identified near existing benchmarks.

4.5. Deformation Measurement Comparison

To highlight the ability of SqueeSAR to detect long term trends, average time series for a sample of the areas outlined in Figure 17 (AOI & Caverns 3 and 115) have been created using survey data projected along the satellite's line of sight. The results of the 8-day CSK data were then overlaid on the benchmark data by introducing a vertical offset in order to match the two measurement trends (Figure 42 to Figure 44).

4.5.1. Average Time Series

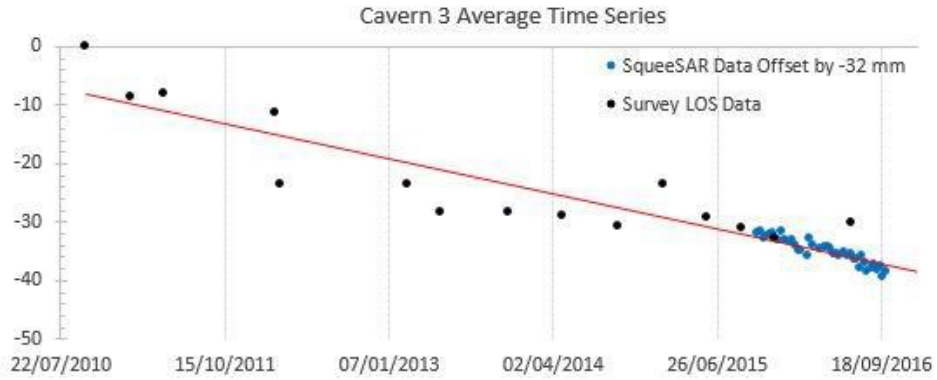

Figure 42: Average time series for all measurement points identified within Cavern 3 (Figure 17) for 8-day CSK SqueeSAR results and ground survey measurements.

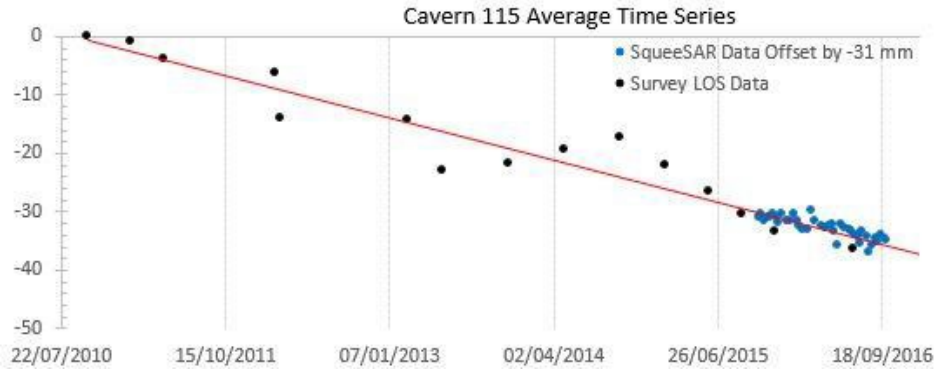

Figure 43: Average time series for all measurement points identified within Cavern 115 (Figure 17) for 8-day CSK SqueeSAR results and ground survey measurements.

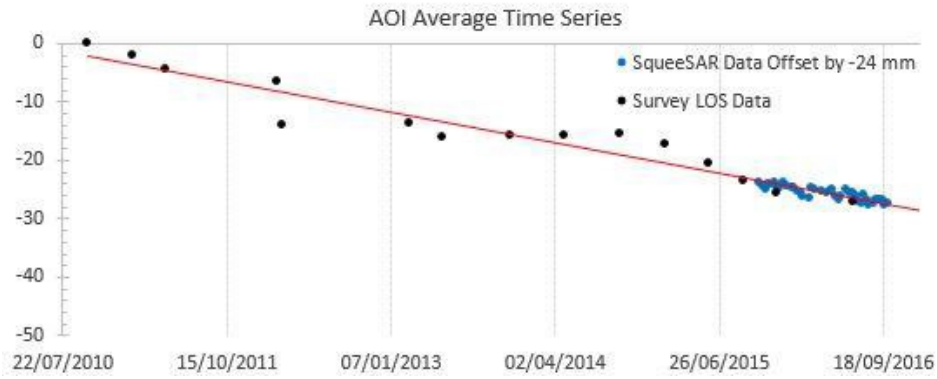

Figure 44: Average time series for all measurement points identified within the AOI (Figure 17) for 8-day CSK SqueeSAR results and ground survey measurements.

4.5.2. Measurement Method Comparison

Annual surface displacement obtained from both SqueeSAR and ground survey methods can be seen in Figure 45. Table 6 summarizes the annual surface displacement values for the SqueeSAR results and the projected ground-based survey results for all well locations. On average, SqueeSAR results show an additional -0.7 mm/year of subsidence over wells. Well locations have been estimated from an unknown local coordinate system, which may affect the accuracy of this comparison. SqueeSAR values over the wells were extracted from a kriged interpolation of the 8-day CSK results. Comparison of measurement methods should be undertaken with these caveats in mind.

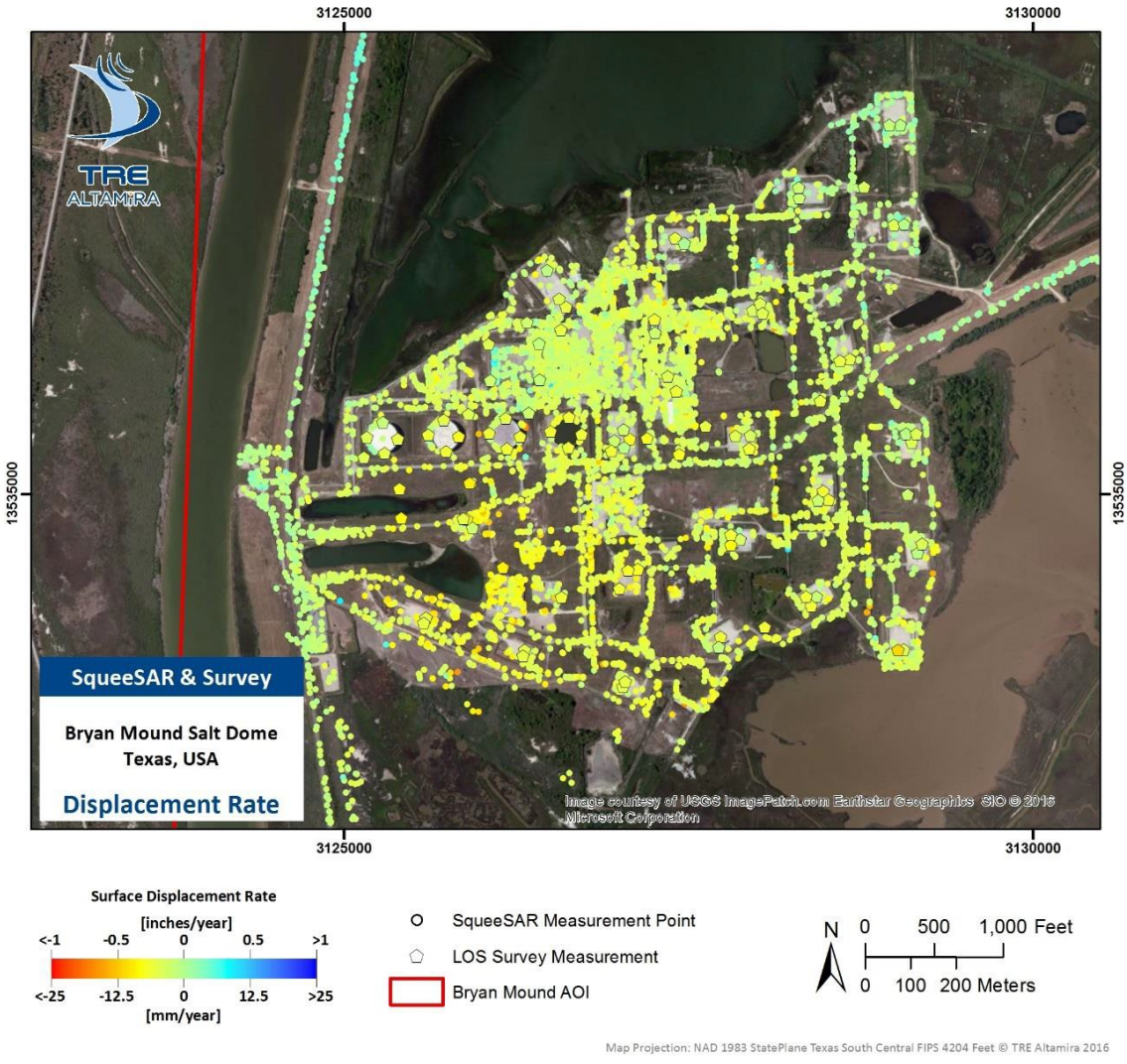

Figure 45: Annual surface displacement results obtained from the 8-day CSK analysis overlaid with annual surface displacement rates of survey measurements projected to the satellite's LOS.

Location	Displacement Rate of Survey Data Projected Along LOS (mm/year)	Displacement Rate of SqueeSAR Data Interpolation (mm/year)	Difference in Measurements (SqueeSAR - Survey) (mm/year)
Well-1	-3.36	-4.06	-0.70
Well-2	-7.40	-4.78	2.62
Well-3	-2.07	-7.15	-5.07
Well-4A	-2.61	-3.73	-1.13
Well-5C	-0.47	-3.49	-3.02
Well-101C	0.43	-2.64	-3.07
Well-102B	-2.72	-0.91	1.81
Well-103C	-0.19	0.15	0.35
Well-104A	-3.32	-2.98	0.35
Well-105C	-5.50	-3.34	2.16
Well-106A	-0.11	-2.88	-2.77
Well-107C	-2.34	-2.59	-0.25
Well-108B	-0.73	-0.82	-0.09
Well-109A	-1.83	-4.07	-2.24
Well-110A	-3.11	-5.21	-2.11
Well-111B	-0.29	0.53	0.82
Well-112C	-1.80	-4.36	-2.56
Well-113A	-4.67	-2.83	1.84
Well-114A	-5.68	-4.73	0.94
Well-115A	-5.93	-6.28	-0.35
Well-116A	-5.87	-8.05	-2.18
Average	**-2.84**	**-3.53**	**-0.70**

Table 6: Differences in displacement rates between the SqueeSAR results and ground survey measurements for well pads.

5. Delivery of Data

The SqueeSAR™ vector data are delivered in a shapefile format and projected in NAD83 State Plane Texas South Central coordinates. The shapefile of each elaboration contains details about the measurement points identified, including displacement rate, elevation, displacement and quality index.

TRE Altamira provides its Clients with a toolbar for ESRI® ArcGIS 10.X that allows the final users to easily load, visualize and analyse the SqueeSAR™ results. For set-up procedure and functionalities, see the attached manual *ToolbarSetup_….pdf*.

Please note that results can be also visualized and downloaded from the TREmaps web-based portal (https://tremaps.treuropa.com). SqueeSAR™ results are superimposed onto a Google Maps background and time-series can be loaded on mouse click. The access to the data is through a secure Client login (only authorised users will have access to the SqueeSAR™ results).

For TREmaps functionalities see: http://tre-altamira.com/tremaps/getting-started/.

The complete list of delivered data is reported in Table 7.

Description	File name
Height, velocity, velocity standard deviation, acceleration, acceleration standard deviation, coherence and time series of all the PS identified in the 8-day CSK analysis (units in mm and inches)	BRYAN_MOUND_8DAYS_CSK_T199_A_I10395A1S_NAD83.shp
	BRYAN_MOUND_8DAYS_CSK_T199_A_I10395A1S_NAD83_Imperial.shp
Height, velocity, velocity standard deviation, acceleration, acceleration standard deviation, coherence and time series of all the PS identified in the 16-day CSK analysis (units in mm and inches)	BRYAN_MOUND_16DAYS_CSK_T199_A_I10395A2S_NAD83.shp
	BRYAN_MOUND_16DAYS_CSK_T199_A_I10395A2S_NAD83_Imperial.shp
Height, velocity, velocity standard deviation, acceleration, acceleration standard deviation, coherence and time series of all the PS identified in the 12-day SNT analysis (units in mm and inches)	BRYAN_MOUND_SNT_T143_D_NAD83_I10395A3S_NAD83.shp
	BRYAN_MOUND_SNT_T143_D_I10395A3S_NAD83_Imperial.shp
Technical Report	BryanMound_SqueeSAR_TechnicalReport2016.pdf

Surface profile animation of Cavern 3 (8-day CSK dataset)	CS_Cavern3_CSK8Day.gif
Surface profile animation of Full Salt Dome (8-day CSK dataset)	CS_AOI_CSK8Day.gif
Surface displacement rate and cumulative deformation (8-day CSK) at benchmark locations (units in millimetres and inches)	Benchmark_CSK8DaySqueeSAR_20161201.csv
Surface displacement rate and cumulative deformation (16-day CSK) at benchmark locations (units in millimetres and inches)	Benchmark_CSK16DaySqueeSAR_20161201.csv
Surface displacement rate and cumulative deformation (12-day SNT) at benchmark locations (units in millimetres and inches)	Benchmark_SNT12DaySqueeSAR_20161201.csv
8-day CSK Dataset animation of surface displacement over time	CSK8Day_CumulativeDisplacementAnimation_2016.gif
16-day CSK Dataset animation of surface displacement over time	CSK16Day_CumulativeDisplacementAnimation_2016.gif
12-day SNT Dataset animation of surface displacement over time	SNT12Day_CumulativeDisplacementAnimation_2016.gif
ESRI ArcGIS map document containing all SqueeSAR data and AOI shapefile (in version 10.4 and version 10.0)	BryanMound_SqueeSAR2016.mxd
	BryanMound_SqueeSAR2016_v10.mxd
ESRI® ArcGIS 10.1 Toolbar	ToolbarTRECustomer….esriAddIn
	ToolbarSetup_….pdf

Table 7: List of delivered files.

The attribute information associated within the database files (dbf) are described in Table 8.

Field	Description
CODE	Measurement Point (MP) identification code
HEIGHT	Topographic Elevation [m] and [ft] referred to WGS84 ellipsoid
H_STDEV	Height standard deviation [m] and [ft]
VEL	MP displacement rate. Positive values correspond to motion *toward the satellite;* negative values correspond to motion *away from the satellite* [in/year] and [mm/year]
V_STDEV	Displacement rate standard deviation [in/year] and [mm/year]
ACC	Acceleration rate [in/year^2] and [mm/year^2]
A_STDEV	Acceleration rate standard deviation [in/year^2] and [mm/year^2]
COHERENCE	Quality measure [between 0 and 1]
Dyyyymmdd	Series of columns that contain the displacement values of successive acquisitions relative to the first acquisition available. Displacement values are expressed in [in] and [mm]

Table 8: Description of the fields contained in the database of single geometry vector data.

6. Summary

TRE Altamira carried out three SqueeSAR analyses over the Bryan Mound salt dome in Texas, USA using three separate datasets:

- A 1-year data stack consisting of 40 images obtained by the CSK satellite on an 8-day acquisition repeat, collected between October 2015 to October 2016;
- An 11-month data stack including 23 images obtained by the CSK satellite on a 16-day acquisition repeat, collected between October 2015 to September 2016; and
- An 11-month data stack of 25 images obtained by the SNT satellite on a 12-day acquisition repeat, collected between December 2014 to November 2015.

The results obtained from the SqueeSAR analyses suggest that most of the salt dome is subsiding, with the strongest subsidence rates identified in the area surrounding cavern 3. Cumulative displacement values ranging from +0.5 inches (+12.5 mm) to -0.7 inches (-18.2 mm) were identified from the 8-day CSK data set, which also produced the highest density of measurement points. The average displacement rate across the entire AOI was -0.1 inches/year (-3.3 mm/year), which is consistent with subsidence rates previously reported from ground surveys.

The average precision of the measurements obtained from the analysis of the CSK and SNT image stacks was ±0.06 inches/year^2 (±1.4 mm/year^2) and ±0.1 inches/year^2 (±2.8 mm/year^2), respectively. This difference is most likely due to the wavelengths of the CSK (3.1 cm) and SNT (5.6 cm) sensors. The smaller wavelength of the CSK satellite often results in a slightly higher associated precision.

The processing extent for the SqueeSAR analyses covers a similar area to that used for the ground-based surveying. Documents summarizing surface displacement rates identified at each benchmark location have been provided as separate files along with this report to facilitate data comparison.

Appendix 1: Additional Properties of the SqueeSAR results over Bryan Mound

Radar Data Acquisition Geometry

InSAR-based approaches measure surface displacement on a one-dimensional plane, along the satellite line-of-sight (LOS). The LOS angle varies depending on the satellite and on the acquisition parameters while another important angle, that between the orbit direction and the geographic North, is nearly constant.

CSK images for the present analysis were acquired from an ascending orbit (satellite travelling from south to north and imaging to the east) (Figure 47); SNT images were acquired from a descending orbit (satellite travelling from north to south and imaging to the west) (Figure 46). The symbol Θ (theta) represents the angle the LOS forms with the vertical and δ (delta) the angle formed with the geographic north. Table 9 lists the values of the angles for this study.

Satellite	Symbol	Angle
SNT	δ	11.94°
	θ	33.92°
CSK	δ	9.35°
	θ	35.05°

Table 9: Satellite viewing angles for the descending orbit imagery sets.

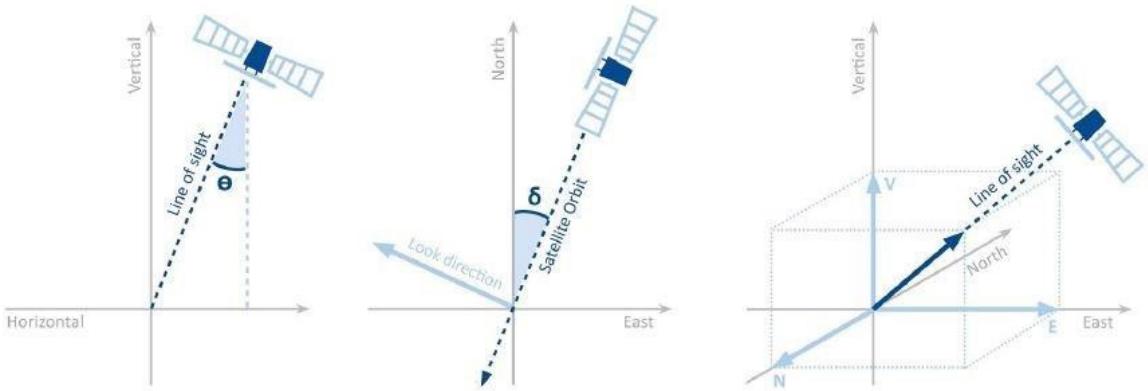

Figure 46: Geometry of the SNT acquisitions over Bryan Mound.

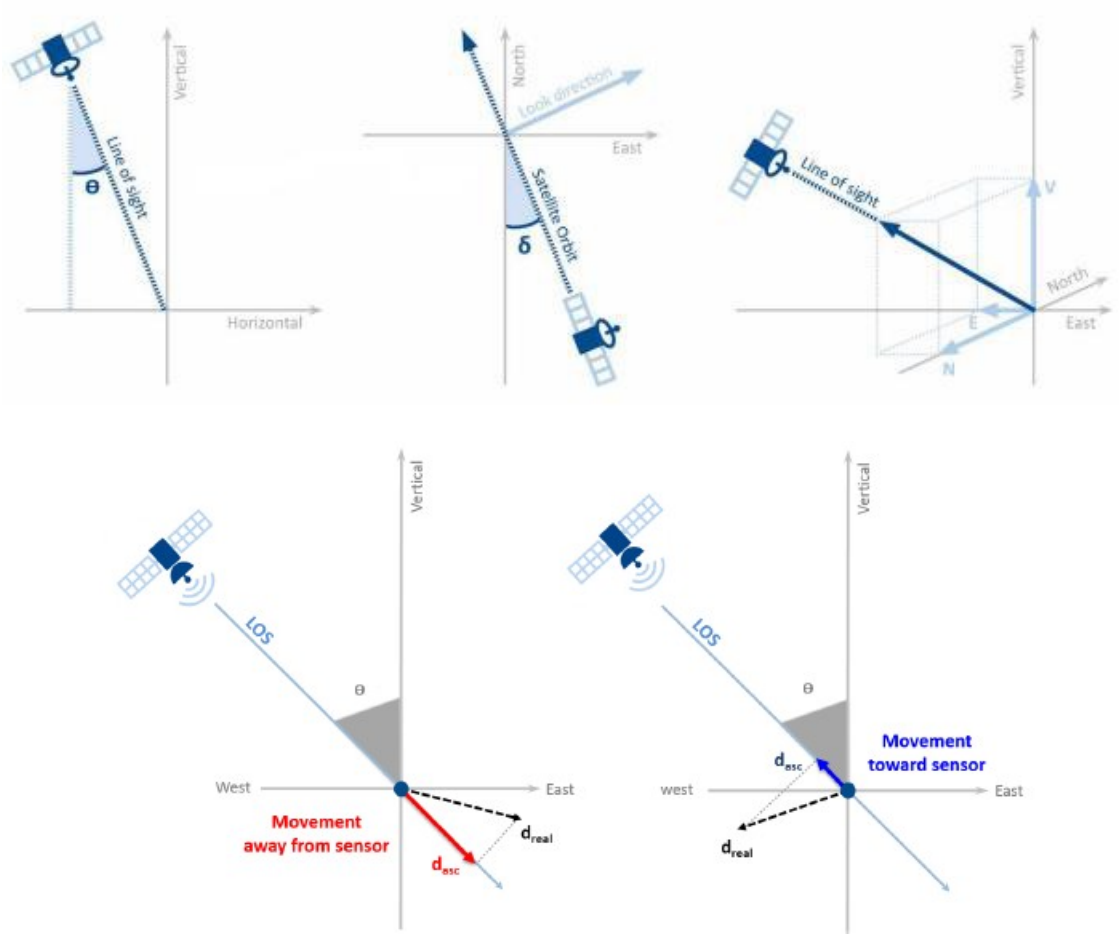

Figure 47: Geometry of the CSK acquisitions over Bryan Mound.

Data Processing

Measurement points were obtained from existing features across the Bryan Mound field, including buildings, wellheads, and other man-made structures. Natural features such as rocks and exposed ground corresponding to large areas (up to hundreds of square meters) also form the basis of many measurement points. It is important to consider that all points are represented as individual points in the GIS environment for clarity of presentation and ease of interpretation.

Table 10 to Table 12, shown below, provides a summary of the other properties relative to the data processing.

Satellite	Cosmo-SkyMed
Acquisition geometry	Ascending
Analysis time interval	17 October 2015 – 03 October 2016
Number of scenes processed	40
Projection system used / datum	NAD83 State Plane Texas South Central
Reference Point location	3,157,843.445 406,328.610
Area of interest	1.65 mi^2 (4.28 km^2)
Number of Measurement Points	7811
Average point density	4733.9 points/$mile^2$ (1820.7 points/km^2)

Table 10: Statistics of the 8-day CSK data set.

Satellite	Cosmo-SkyMed
Acquisition geometry	Ascending
Analysis time interval	17 October 2015 – 25 September 2016
Number of scenes processed	23
Projection system used / datum	NAD83 State Plane Texas South Central
Reference Point location	3,157,851.258 406,333.818
Area of interest	1.65 mi^2 (4.28 km^2)
Number of Measurement Points	5058
Average point density	3065.5 points/$mile^2$ (1181.8 points/km^2)

Table 11: Statistics of the 8-day CSK data set.

Satellite	Sentinel
Acquisition geometry	Descending
Analysis time interval	26 December 2014 – 03 November 2015
Number of scenes processed	25
Projection system used / datum	NAD83 State Plane Texas South Central
Reference Point location	3,158,028.341 406,516.110
Area of interest	1.65 mi^2 (4.28 km^2)
Number of Measurement Points	736
Average point density	446.1 points/$mile^2$ (172.0 points/km^2)

Table 12: Statistics of the 12-day SNT data set.

Standard Deviation and Precision

Standard deviation values of the displacement measurements are a function of the factors listed below and of local ground movement dynamics.

- Spatial density of the PS and DS (higher densities produce higher precisions)
- Quality of the radar targets (signal-to-noise ratio levels)
- Distance from the reference point
- Number of images processed and period of time covered by the imagery
- Climatic conditions at the time of the acquisitions
- Distance between the measurement point and the reference

In addition to each measurement point having an associated standard deviation value to represent the error of the displacement measured, results can also be characterized by the accuracy of the technique. Specifically, three parameters are used to characterize the overall accuracy of the results:

- Precision of the estimated deformation rates;
- Precision of the estimated elevations;
- Precision of the geocoding.

Table 13 summarizes the typical precision values applicable to PS located within 2 km from the reference point when **at least 45 radar images** have been processed.

DEFORMATION RATE	< 1 [mm/yr]
DISPLACEMENT ERROR (single displacement between contiguous satellite images)	< 5 [mm]
ELEVATION	± 1.5 [m]
POSITIONING ERROR ALONG EAST DIRECTION	± 3 [m]
POSITIONING ERROR ALONG NORTH DIRECTION	± 2 [m]

Table 13: Measurement accuracies for PS located within 2 km of the reference point, based on the processing of at least 45 SAR images.

Appendix 2: InSAR Processing

InSAR

Interferometric Synthetic Aperture Radar, also referred to as SAR interferometry or InSAR, is the measurement of signal phase change (interference) between radar images. When a point on the ground moves, the distance between the sensor and the point changes, thereby producing a corresponding shift in signal phase. This shift is used to quantify the ground movement.

An interferogram is a 2D representation of the difference in phase values. Variations of phase in an interferogram are identified by fringes, colored bands that indicate areas where and how much movement is occurring. The precision with which the movement can be measured is usually in the centimetre (cm) range as the phase shift is also impacted by topographic distortions, atmospheric effects, and other sources of noise.

DInSAR

When InSAR is used to identify and quantify ground movement the process is referred to as Differential InSAR (DInSAR). In DInSAR topographic effects are removed by using a DEM of the area of interest to create a differential interferogram. Differential InSAR is still impacted by atmospheric effects, as there is no method for removing this signal phase contribution. It is a useful tool for identifying footprints of progressing movement and creating deformation maps. The limitations of DInSAR are its relatively low precision (cm scale) and that it cannot distinguish between linear and non-linear motion.

PSInSAR™

Permanent Scatterer SAR Interferometry is an advanced form of DInSAR. The fundamental difference is that it uses multiple interferograms created from a stack of at least 15 radar images.

Permanent Scatterer SAR Interferometry was developed to overcome the errors produced by atmospheric artifacts on signal phase. The PSInSAR algorithm automatically searches the interferograms for pixels that display stable radar reflectivity characteristics throughout every image of the data set. In PSInSAR these pixels are referred to as Permanent Scatterers (PS). The result is the identification of a sparse grid of point-like targets on which an atmospheric correction procedure can be performed. Once these errors are removed, a history of motion can be created for each target, allowing the detection of both linear and non-linear motion.

The result is a sparse grid of PS that are color-coded according to their deformation rate and direction of movement. The information available for each PS includes its deformation rate, acceleration, total

deformation, elevation, coherence as well as a time series of movement. The PSInSAR algorithm measures ground movement with millimetre accuracy.

SqueeSAR™

Permanent Scatterers are objects, such as buildings, fences, lampposts, transmission towers, crash barriers, rocky outcrops, etc., that are excellent reflectors of radar microwaves. However, TRE has noticed that many other signals are present in the processed data. These do not produce the same high signal-to-noise ratios of PS but are nonetheless distinguishable from the background noise. Upon further investigation it was found that the signals are reflected from extensive homogeneous areas where the back-scattered energy is less strong, but statistically consistent. These areas have been called distributed scatterers (DS) and correspond to rangeland, pastures, bare earth, scree, debris fields, arid environments, etc. (Figure 48).

The SqueeSAR algorithm was developed to process the signals reflected from these areas. As SqueeSAR incorporates PSInSAR no information is lost and movement measurement accuracy is unchanged.

The SqueeSAR algorithm also produces improvements in the quality of the displacement time series. The homogeneous areas that produce DS normally comprise several pixels. The single time series attributed to each DS is estimated by averaging the time series of all pixels within the DS, effectively reducing noise in the data.

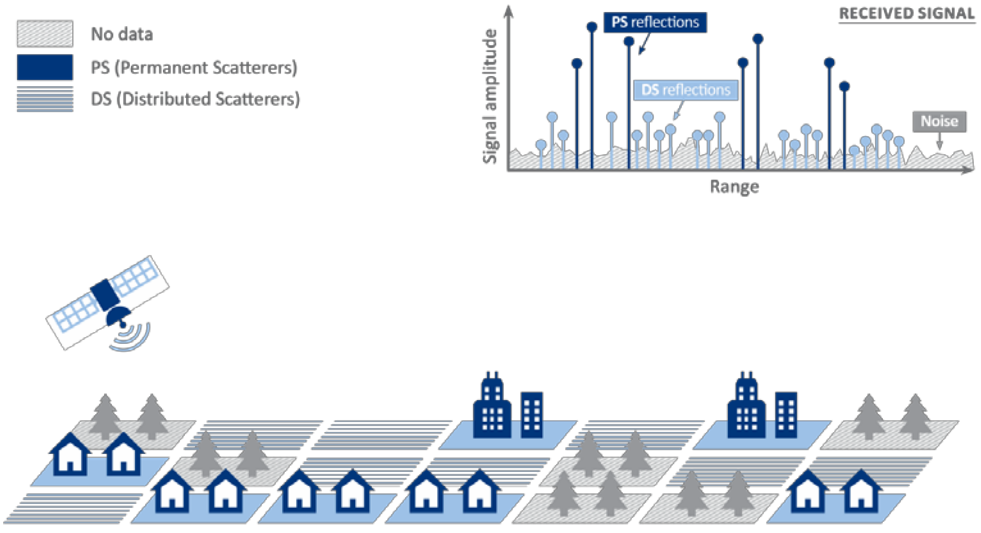

Figure 48: Illustration of the identification of permanent (PS) and distributed scatterers (DS) by the SqueeSAR algorithm.

Appendix 3: Data Processing

Methodology

The identification of PS and DS in a series of radar images comprises a sequence of steps.

First, all radar data archives are screened to determine the most suitable source of raw data for the particular area of interest and to select all the high-quality images within the chosen data set.

As the signal echo from a single point target contains many returning radar pulses it appears defocused in a synthetic aperture radar (SAR) raw image. The first processing step is therefore to focus all the received energy from a target in one pixel. The images are then precisely aligned to each other, or co-registered, and analyzed for their suitability for interferometry. The parameters that are analyzed are the normal baseline and the temporal distribution of the images.

There then follows a number of statistical analyses on the phase and amplitude characteristics of the backscattered radar signal that return to the satellite. If a concentrated number of signals reflect off a particular feature within a pixel and backscatter to the satellite, the feature is referred to as a 'scatterer'. When the same scatterer appears in all, or most, of a data set of SAR images of a particular location, then the scatterer is deemed to be 'permanent'.

At this stage, it is possible to identify a subset of pixels, referred to as Permanent Scatterer Candidates (PSC), that are used to estimate the impact on signal phase of ionospheric, tropospheric and atmospheric effects, as well as possible orbit errors. Once the signal phase has been corrected for these effects, any remaining changes in signal phase directly reflect ground movement.

Master Image Selection

SqueeSAR requires that one image (or scene) in each data set has to become both a geometric and temporal reference to which all the other images are then related. This image is referred to as the master image and those that remain are slave images.

The master image should be chosen according to the following criteria:

- it minimizes the spread of normal baseline values for the slave images;
- similarly, it minimizes the temporal baseline values between the master and each slave image; and
- it minimizes the effects of signal noise arising from changes in vegetation cover and/or small changes in the look angle of the satellite from one scene to another.

Signal Phase and Amplitude Analysis

General

Each pixel of a SAR image contains information on the amplitude of signals that are backscattered toward the satellite, as well as on the signal phase. The amplitude is a measure of the amount of the radar pulse energy reflected, while the phase is related to the length of the path of the electromagnetic wave, from the platform to the ground and back again.

Analyses of both amplitude and phase of the SAR image provide an indication of the stability of each pixel, over time, whereby it is possible to identify those pixels that are most likely to behave as Permanent Scatterers. Statistical methods are used extensively in this process.

Among the different statistical parameters that can be computed two are of particular interest: the Phase Stability Index (PSI), obtained from the phases of the images within the data set, and the Multi Image Reflectivity (MIR) map, derived from the amplitude values of the available acquisitions.

Radar phase and coherence

In standard SqueeSAR analyses, the phase stability is strongly linked to the concept of coherence. Pixels that consistently display high phase stability are said to be coherent. Coherence is measured by an index that ranges from 0 to 1. When a pixel is completely coherent, it will have a coherence value of 1. Correspondingly, if a pixel has a low phase stability, its coherence index will be 0. In general, interferometry is successful when the coherence index lies between 0.5 and 1.0.

Radar amplitude and multi-image reflectivity

The amplitude of a pixel within a SAR image is the aggregate of the backscattered energy toward the satellite from within the pixel's equivalent land area. This equivalent land area is referred to as the radar resolution, and in the case of the ERS and RSAT satellites, it measures about 20 m by 4 m, and 7 m by 5 m, respectively. It is necessary to look into the amplitude values of all the images in the data set, in order to understand exactly what was seen by the satellite at the time of each acquisition.

If a target has experienced significant change in its surface characteristics it will exhibit variation in its reflectivity (electromagnetic response) between two acquisitions. In such circumstances, the possibility of detecting movement by means of SAR interferometry is seriously compromised. The signal phase difference between the two images now contains not only the contribution due to displacement, but also that due to the change in the reflectivity of the target. This prevents, in the worst case, the obtaining of any useful information on ground movement.

Accordingly, it is necessary to look into the amplitude values of all the images in the data set, in order to understand exactly what was seen by the satellite at the time of each acquisition.

Another artifact linked to amplitude is known as speckle. Speckle is random noise that appears as a grainy salt and pepper texture in an amplitude image. This is caused by random interference from the multiple scattering returns that occur within each resolution cell. Speckle has an adverse impact on the quality and usefulness of SAR images. However, the higher the number of images taken of the same area at different times or from slightly different 'look' angles, the easier it is to reduce speckle. This increases the quality and level of details of the amplitude image enabling it to be used as a background layer for observing the presence of PS results.

The Multi Image Reflectivity (MIR) map is the means by which speckle reduction is accomplished. Averaging a number of images tends to negate the random amplitude variability, leaving the uniform amplitude level unchanged.

It should be emphasised that the information in the MIR map is the reflectivity of each pixel, i.e. the ability to backscatter the incident wave toward the satellite. Flat surfaces (roads, highway, rivers, lakes) act like a mirror, meaning that if their orientation is not exactly perpendicular to the incident wave negligible energy is reflected back to the sensor; they appear dark in the image. On the other hand, because of their irregular physical shape, metal structures or buildings reflect a significant portion of the incident signal back to the radar, resulting in very bright pixels in the MIR map.

Interferograms

After the statistical analyses of the SAR images have been completed, a set of differential interferograms is generated. This entails subtracting the phase of each slave image from the phase of the master image. In doing so, the difference in signal path length between the two images is calculated. This difference is related to possible ground motion.

In any SAR image, there are embedded topographic distortions that arise during image acquisition. These are removed using a reference Digital Elevation Model (DEM), leaving ground movement and the signal phase distortions arising from atmospheric effects as the only embedded variables.

The differential interferograms represent the starting point for applying the PSInSAR approach.

Estimation of the Atmospheric Effects

When a radar signal enters and exits a moisture-bearing layer in the atmosphere, its wavelength can be affected, introducing potential errors into the signal path length. The removal of atmospheric impacts is fundamental for increasing the precision of ground movement measurement.

A sub-set of pixels, usually corresponding to buildings, lampposts, antennas, small structures and exposed rocks, is chosen from among those that have high PSI values. These are referred to as PS Candidates (PSC). PSC density is, of course, higher in towns and cities rather than in forests and vegetated areas. However, it is often possible to obtain good PSC density in rural areas.

For each image, the atmospheric impacts are estimated at each PSC location. The process is statistically based and benefits in accuracy by the greater the number of available images for the analysis. By comparing the atmospheric contribution on neighboring pixels that would be experiencing the same atmospheric conditions, the atmospheric contribution can be reconstructed over the whole image.

The processed data set allows identification of a PSC cluster dense enough to identify and extract the atmospheric contribution over the entire area of interest.

Post-processing

In this stage the processed data undergoes a thorough quality control following ISO 9001:2000 guidelines. The PS data is checked for anomalies, aligned on an optical image layer usually provided by the client and the final report is prepared.

Appendix 4: Acronyms and abbreviations

AOI	Area Of Interest
DEM	Digital Elevation Model
DInSAR	Differential Interferometric SAR
DS	Distributed Scatterer(s)
GIS	Geographic Information System
InSAR	Interferometric SAR
LOS	Line Of Sight
PS	Permanent Scatterer(s)
PSInSAR	Permanent Scatterers SAR Interferometry is a world-wide POLIMI Trademark
SAR	Synthetic Aperture Radar
SqueeSAR	The most recent InSAR algorithm patented by TRE
TRE	Comprehensive term for Tele-Rilevamento Europa and TRE Altamira
TS	(Permanent Scatterer Displacement) Time Series

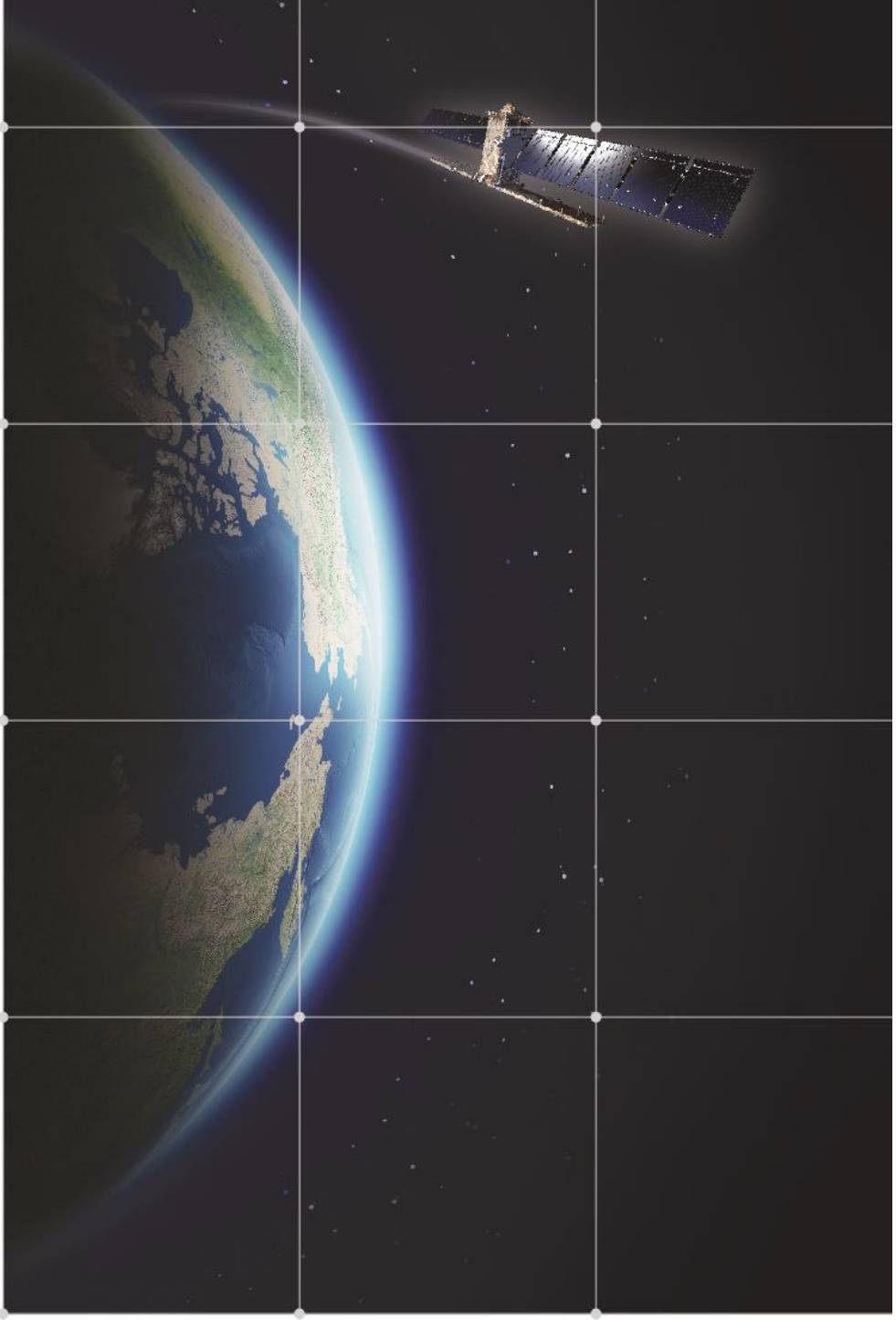

TRE
ALTAMIRA
A CLS Group Company

MILAN

Ripa di Porta Ticinese, 79
20143 Milano - Italy
Tel. +39.02.4343.121
Fax +39.02.4343.1230

BARCELONA

C/ Corsega, 381-387
E-08037 Barcelona Spain
Tel.: +34 93 183 57 50
Fax: +34 93 183 57 59

VANCOUVER

410 - 475 West Georgia Street
Vancouver, BC V6B 4M9 - Canada
Tel. +1.604.331.2512
Fax +1.604.331.2513

tre-altamira.com

DISTRIBUTION

Electronic copies to:

1 Wayne Elias (wayne.elias@hq.doe.gov)
for distribution to DOE SPR Program Office, Washington, D.C.
U.S. Department of Energy
Office of Fossil Energy
Forrestal Building
1000 Independence Ave, SW
Washington, D.C. 20585

1 Diane Willard (diane.willard@spr.doe.gov)
for distribution to DOE SPR Project Management Office, New Orleans, LA.
U.S. Department of Energy
Strategic Petroleum Reserve Project Management Office
900 Commerce Road East
New Orleans, LA 70123

1	MS0735	Leigh Cunningham	8862
1	MS0735	Erik Webb	8860
1	MS0750	Carolyn Kirby	8863

1	MS0899	Technical Library	9536 (electronic copy)


Sandia National Laboratories